Multiple generations of granitoid gneisses hosting supracrustal belts in the Archean Inukjuak domain (Québec, Canada)

Jennika Greer

Department of Geological Sciences, University of Colorado, Boulder

Defended November 5, 2013

Thesis Advisor
Stephen J. Mojzsis, Department of Geological Sciences

Committee Members
Stephen J. Mojzsis, Department of Geological Sciences
Nicole L. Cates, Department of Geological Sciences
Charles Stern, Department of Geological Sciences
Carol Cleland, Department of Philosophy

Abstract. The Inukjuak domain in the northwestern Superior Province of Canada hosts numerous supracrustal belts that occur as km-scale enclaves in Archean granitoid gneisses. The Eoarchean (ca. 3750-3780 Ma) Nuvvuagittuq Supracrustal Belt (NSB) in northern Québec is the best known of these variably metamorphosed and deformed volcano-sedimentary (supracrustal) units. These Innucsuac Complex supracrustals are dominantly amphibolitic, and are surrounded and/or intruded by several generations of granitoid gneisses of tonalite-trondhjemite-granodiorite (TTG) composition. Few detailed geochronology studies for the assorted Inukjuak domain gneisses and the associated enclaves have been performed. A tonalitic gneiss at the margin of the NSB fold belt was previously assigned a ca. 3650 Ma age, and granitoid gneisses of the surrounding Boizard suite (A_{boi}), were considered to have formed at about 2700 Ma. We report new major-, minor- and trace element geochemistry coupled with U-Pb zircon geochronological data for these various gneisses as well as from a little-studied, locally significant gneiss (the Voizel suite; A_{voi}). Results show that a tonalitic gneiss at the center of the NSB fold belt (Central Tonalitic Gneiss; CTG) preserves mainly ca. 3650 Ma zircon cores. Outside the NSB, the previously undated 3550 Ma A_{voi} that was thought to be contemporaneous with the CTG is instead about 100 Myr younger. A_{boi} rocks contain inherited zircon cores up to 3700 Ma with ca. 2700 Ma rim overgrowths. A tonalitic gniess that transects a large unnamed supracrustal belt northeast of the NSB (within A_{voi}), yielded a maximum concordant zircon age of 3653±8 Ma.

1. Introduction

Supracrustal belts comprise deformed km-scale volcano-sedimentary enclaves that are locked within ancient granite-granitoid gneiss terranes (de Witt and Ashwall, 1995). Ranging in size from meters to tens of kilometers in outcrop, Eoarchean (3.6-3.85 Ga) supracrustal enclaves (*sensu stricto*) are found on all the continents and all are captured within younger tonalite-trondhjemite-granodiorite (TTG) gneiss complexes. These TTG gneisses are separated from the surrounding cratonic geology by shear zones. The events that led to the juxtaposition of the TTG gneisses also resulted in the metamorphism and deformation of the supracrustal units themselves. Despite the fact that these rocks tend to be strongly altered due to residence times in the crust of upwards of several billion years, they nevertheless constitute the best sources of evidence for the early geochemical and biological evolution of Earth. To unravel the metamorphic history of these supracrustal enclaves requires detailed analysis of the geology, age and origin of the encompassing gneisses.

The ca. 3750-3780 Ma Nuvvuagittuq supracrustal belt (NSB) in northern Québec is one such enclave. It is important to note that the NSB, however, is merely the best known of about a dozen km-scale enclaves. Collectively they are termed the *Innucsuac Complex* that in turn is part of the Innukjuak domain of the Northwest Superior Province in Canada (Fig. 1a; Simard et al., 2003; David et al., 2003; Stevenson et al., 2005; Cates and Mojzsis, 2007; O'Neil et al., 2007). In this paper, we present new geochemical and U-Pb zircon geochronological data for the Inukjuak TTG gneisses that immediately surround and intrude the NSB and another large (>10 km^2)

supracrustal belt discovered to the northeast of the NSB that is informally termed here as the *Ukalik supracrustal belt* (USB)[1].

2. Geologic Background

The Inukjuak domain is one of several domains in the Hudson Bay Terrain, which is dominated by Neoarchean plutonic suites (Fig 1a; O'Neil et al., 2007). The approximately 8 km^2 outcrop of the NSB has generated enormous interest because of the verified discovery of anomalous deficits in $^{142}Nd/^{144}Nd$ vs. Bulk Silicate Earth (O'Neil et al., 2008; Roth et al., 2013); the anomalous $^{142}Nd/^{144}Nd$ value in conjunction with ancient model ages have led some to propose that it may be as old as 4300-4400 Ma (O'Neil et al., 2008; 2012). The NSB rocks are the only part of the region that has been studied in the detail adequate to understand a complex and protracted geologic history (Cates et al., 2013). The Nuvvuagittuq belt is composed mostly of basaltic amphibolites, layered ultramafic schists that include rocks with geochemical signatures similar to komatiites (Cates and Mojzsis, 2007; Frank et al. *in preparation*), finely banded quartz magnetite (banded iron-formation) and quartz-biotite schists (Simard et al., 2003; Cates and Mojzsis, 2007; O'Neil et al., 2007; David el al., 2009). Detrital zircons of igneous origin in quartzites along with ages for igneous zircons from trondhjemitic gneisses that cross-cut the supracrustal sequences indicate that the NSB formed at ca. 3800 Ma (Cates and Mojzsis, 2007; David et al., 2009; Cates et al., 2013).

Many other small (<1m) enclaves, as well as large (>1 km) supracrustal belts have been provisionally mapped to exist within the Innukjuak domain, including the *Ukalik* rocks. Unlike the Nuvvuagittuq outcrops, the USB is more strongly deformed into a set of relatively small disconnected mafic to ultramafic enclaves with very minor (<1% of total outcrop)

[1] "Ukalik," Inuktitut for "artic hare," is a name that has not yet been endorsed by the Pituvik Landholding Corporation nor by the local government council and is simply meant as an informal name for a suite of supracrustal rocks that appear to have previously been part of a larger a coherent unit.

metasedimentary components that range in size from 1-20 m. Altogether, the Ukalik enclaves are surrounded and extensively intruded by a group of strongly foliated felsic grey gneisses of the Voizel suite (Simard et al., 2003). An earlier report by David et al. (2009) documented a ca. 3660 Ma U-Pb zircon ages by LA-ICP-MS and ID-TIMS for a single gneiss sample collected at the northwest margin of the NSB, which was attributed by them to the Voizel suite (A_{voi}). Zircons from a second sample from the gneisses at the core of the NSB, which the authors also tentatively assigned to Voizel suite, yielded metamorphic ages of ca. 2700 Ma.

Voizel suite rocks are surrounded and disrupted by a pinkish granitoid with only slight tectonic fabric named the Boizard suite (Simard et al., 2003) that was previously assigned an age of 2750 ± 5 Ma. Published reports show some evidence that the Boizard suite (A_{boi}) intrudes into the various supracrustal enclaves; a pegmatitic dike of this age was described within the NSB (Simard et al., 2003). The abundant number of metamorphic zircon growth ages at about 2700 Ma indicates that the emplacement of the Boizard suite appears to have led to regional metamorphism of the complex (Cates and Mojzsis, 2007, 2009; Cates et al., 2013).

3. Methods

Representative samples were collected during the course of regional-scale field mapping of the various gneisses associated with the NSB and USB (Fig. 1b). A subset of these samples were chosen for geochemical analyses based on their apparent lack of weathering, homogeneity at the hand-sample scale, and the likelihood of producing abundant zircons for geochronology.

3.1. Whole-rock Geochemistry

Samples for whole-rock geochemistry were crushed to fine powders at the Rock Preparation Facility of the Department of Geological Sciences at the University of Colorado. Ceramic mortars were pre-cleaned with washed quartz sand and conditioned with small amounts of

sample before powders were made of the main sample masses. Care was taken to avoid any contact of the samples with metal hammers, saws and other dividing apparatus that could compromise future analytical work. Splits from homogenized powders were subdivided for major-, minor-, and trace element geochemistry and for archival purposes. Whole rock geochemical analyses were performed at the Centre de Recherches Pétrographiques et Géochimiques (CRPG) SARM Facility in Nancy (France).

3.2. Ion microprobe geochronology

A subset of each sample was set aside for zircon extraction. Whole rock samples were crushed and sieved to <350 μm. Sieved aliquots were then passed through two stages of standard heavy liquid separations (Tetrabromoethane and Methylene Iodide) and subsequently rinsed in reagent-grade acetone. After drying, gross magnetic minerals fractions were removed via hand-magnet, followed by a separation with a Franz magnetic separator. Zircon grains from the least magnetic fraction were handpicked under a binocular microscope, placed on double-sided adhesive tape according to grain size, and cast in 2.52 cm diameter molds with Buehler© epoxide resin. A variety of zircon sizes and morphologies was chosen to diminish sampling bias. The sample mounts were then polished in stages down to 0.25 μm alumina to expose grain centers. Transmitted and reflected optical micrograph mount maps were produced to facilitate identification and navigation on the mounts.

Immediately prior to ion microprobe analysis, the zircon mounts were ultrasonically bathed in a 1N HCl solution for 2 minutes to reduce common Pb contamination, rinsed in ultrapure water, air dried and sputter coated with ~100 Å of Au to facilitate conductivity. All U-Pb zircon ion microprobe geology was determined using the UCLA Cameca *ims*1270 high-resolution ion microprobe under standard operating conditions (e.g. Cates et al., 2013). A summary is provided

here: a ~8 nA O_2^- primary ion beam was defocused to a 25-μm spot and the ion probe was operated at a mass resolving power of ~6000 to exclude molecular interferences. Oxygen flooding to a pressure of 3.2×10^{-5} torr was used to increase Pb^+ yields (Schuhmacher et al. 1994) and ages for unknown zircons were determined by comparison with a working curve defined by multiple measurements of zircon standard AS3 that yields concordant $^{206}Pb/^{238}U$ and $^{207}Pb/^{235}U$ ages of 1099.1±0.5 Ma (Paces et al., 1993; Black et al. 2003). Data were reduced using the program ZIPS, written by C. Coath (University of Bristol). Geochronological data are presented using the Isoplot software package (Ludwig, 2003) by generating Tera-Wasserburg plots ($^{207}Pb/^{206}Pb$ vs. $^{238}U/^{206}Pb$) that yield discordia and weighted average ages.

3.3 Zircon trace element geochemistry

All zircon rare earth element ($[REE]_{zirc}$) analyses were made on the UCLA Cameca *ims*1270 ion microprobe following the approach described by Schmitt and Vazquez (2006). Analysis spots were ~25 μm in diameter and positioned to overlap previous geochronology analysis points. The REE intensities were normalized to $^{30}Si^+$ and corrected for interfering oxides. The trace element content of NIST standard glass 610 was used to determine the analytical sensitivity. Instrument stability was monitored by periodic REE measurements on standard zircon AS3.

4. Results

4.1. Whole-rock Geochemistry

4.1.1. Central Tonalitic Gneiss (CTG)

Rather than constituting a single mass of homogeneous tonalitic gneiss, outcrops of the CTG instead comprise diverse and overlapping gneissic granitoids and biotite-rich bodies with highly variable grain sizes all foliated in a general N-S direction (Fig. 2a). Within the CTG are disrupted and strongly recrystallized rocks that superficially resemble banded iron-formation that has

experienced extreme quartz mobility. Presumably this "BIF" was originally part of the Nuvvuagittuq supracrustal succession before becoming engulfed in the CTG. Two samples both plot compositionally on the border between tonalite and granodiorite on the conventional TTG classification diagram (Fig. 3; Barker, 1979). They show typical (felsic) granitoid REE patterns with chondrite-normalized LREE enrichments around 100, and HREE enrichment of about 10 with weak negative Eu anomalies (0.66- 0.95; Fig. 4). On a multi-element plot, both samples also have typical igneous granitoid patterns with strong negative Nb anomalies (both have Nb/Nb* = 0.13) and moderate Ti anomalies (Ti/Ti* for *IN05001* = 0.58 whereas *IN12012* is 0.48). Sample *IN05001* is also enriched in Zr (Zr anomaly of 1.92; Fig. 5; Table 1).

4.1.2. Voizel Suite (A_{voi})

In outcrop, the coarse-grained A_{voi} rocks appear gray or white, depending on how weathered they are (Fig. 2b). They have a pronounced gneissic texture with a foliation trend that conforms to the structural outline of the USB as seen in satellite photographs. In places, the A_{voi} disrupts and encloses dominantly mafic to ultramafic USB enclaves into meter- to 10-meter scale pods. For this study, five samples were chosen for geochemical analysis. Two samples come from the "upper lobe" and three samples from the "lower lobe" (Fig. 1b.), and these plot in the tonalite, granodiorite, or quartz-monzonite fields on a TTG classification diagram (Fig. 3). On an REE plot, the five samples have typical igneous felsic patterns, with chondrite normalized LREE enrichments around 100 and HREE enrichments around 10. The two A_{voi} samples *IN12050* and *IN12027* that fall in the quartz-monzonite field show large positive Eu anomalies, with Eu/Eu* values of about 2. Samples *IN12050* and *IN12014* have relatively low concentrations of REE overall (<100x chondrite LREE, < 10x chondrite HREE), and are depleted in HREE relative to the other samples analyzed here (Fig. 4). On a multi-element plot, A_{voi} samples show typical

igneous felsic patterns with strong negative Nb anomalies (Nb/Nb* values between 0.05 and 0.51) and moderate Ti anomalies (Ti/Ti* values from 0.28 to 0.70). All five of the samples have positive Zr anomalies, with Zr/Zr* values ranging between 2.65 and 1.12 (Fig. 5; Table 1).

4.1.3. Boizard Suite (A_{boi})

The Boizard is a coarse grained, pinkish, K-feldspar-bearing granite as classified by a TTG classification diagram (Fig. 3) with little or no fabric (Fig. 2c). The A_{boi} rocks enclose the Voizel suite and dominate the gneissic landscape surrounding the different supracrustal belts of the *Innucsuac Complex*. On a REE plot the two A_{boi} samples have typical felsic patterns but differ in their LREE composition: *IN12016* has LREE values around 50, while *IN12054* has chondrite-normalized LREE above 200. The HREE enrichments for these samples are around 10 and both samples exhibit negative Eu anomalies (Eu/Eu* for *IN12016* = 0.71, and for *IN12054* is 0.50; Fig. 4). On a multi-element plot, the A_{boi} samples have typical igneous felsic patterns with strong Nb anomalies (0.29- 0.02) and moderate Ti anomalies (0.48-0.49). Sample *IN12016* has a negative Zr anomaly of 0.46 (Fig. 5; Table 1).

4.1.4. "Ukalik" supracrustal enclaves

Rare, thin (10 cm- to m-scale) banded gray TTG gneisses were documented to transect the amphibolitic USB enclaves, and field relationships suggest that these gneisses pre-date the dismemberment of the previously coherent supracrustal belt by the intruding A_{voi} (Fig. 2d). Three of these cross-cutting gneissic sheets were sampled for analysis and all show typical felsic patterns with chondrite normalized LREE enrichments around 100 and HREE enrichment of about 10. Sample *IN12042* has a moderate positive Eu anomaly (Eu/Eu* = 1.45), while *IN12053* shows a negative Eu anomaly (Eu/Eu* = 0.89; Fig. 4). The three gneisses also have strong

negative Nb anomalies (Nb/Nb* ranging from 0.14 to 0.17), and moderate Ti anomalies (Ti/Ti* ranging from 0.45 to 0.63; Fig. 5; Table 1).

4.2. Geochronology

4.2.1. Central Tonalitic Gneiss

The two samples for which geochemical data were available (*Sec. 4.1.1*) from the CTG were prepared for geochronological analysis. One of these samples was collected from the northeastern margin of the NSB, and the other was taken from the easternmost limit of the NSB (Fig. 1b).

IN12012. A total of 15 spots were analyzed on 15 grains. The weighted average age of the 11 most concordant grains (within 6% of concordia) is 3652 ± 14 Ma (Fig. 6a). These zircon grains are primarily zoned cores surrounded by rims too thin to measure by conventional ion microprobe techniques (Fig. 7). Younger ages, not within 10% of concordance, come from altered cores filled with fractures. The range of Th/U ratios for the concordant and discordant grains is the same and ranges by a factor of 10^2 from 0.08 to 1.80 (Table 2).

IN05001. Analysis of 26 spots on 26 grains yielded an upper intercept age of 3546 ± 86 (Fig. 6b; MSWD = 4.6); however, a weighted average age of the most concordant analyses (within 7.5% concordance) lowers this estimate to 3487 ± 15 Ma. The range of U/Th values for this sample is from 0.063 to 0.63 (Table 2).

4.2.2. Voizel Suite

Five A_{voi} samples from the USB were selected for geochronology (Fig. 1b) that also had whole-rock geochemistry data available (*Sec. 4.1.2*). Two are from the upper lobe (*IN12014, IN12027*) and three are from the lower lobe (*IN12041, -46* and *-50*) .

IN12014. A total of 10 analyses on 10 zircons yielded an upper intercept of 3550^{+52}_{-44} (MSWD = 1.7). Two more zircon grains (4 analyses) from this sample were discordant but trace along a horizontal axis on the Tera-Wasserburg plot, which is suggestive of recent lead loss (Fig. 6c). These four analyses have a weighted average of 1871±86 Ma. The ca. 3550 Ma ages are exclusively from the cores of euhedral to subhedral zircons with obvious younger overgrowths, whereas the younger population ages are exclusively from zircon rims (Fig. 7). The Th/U values for the most concordant analyses (95%) in the oldest population range from 0.06 to 9.6 (Table 2).

IN12027. A total of 15 analyses were made on 12 grains, but only 4 of the grains were found to be within 15% of concordance. A weighted average of these four grains gives an age of 3519 ± 16 Ma (Fig. 6d). The concordant ages come from cores of euhedral to subhedral grains with ca. 3300 Ma rims (Fig. 7). Most of the grains have Th/U ratios that range from 0.2 to 0.5, but the most concordant grain has a ratio of 0.69 (Table 2).

IN12041. We performed 14 analyses on 12 grains that yielded a discordia with an upper intercept of 3550 ± 120 Ma (Fig. 6; MSWD = 4.7). The oldest, most concordant age comes from a zircon core region that is surrounded by a zoned rim overgrowth. Younger ages (zircon 3.1_b, 2175 ± 30 Ma; zircon 4.2, 2580 ± 9 Ma; zircon 3.19, 3161 ± 6 Ma) come from rims or cores with fractures or metamict textures (Fig. 7). The Th/U ratios for these grains ranges from 1.1 to 0.21, and the most concordant grains typically have higher values (Table 2).

IN12046. A total of 23 analyses on 21 grains yielded a discordia with an upper intercept age of 3483 ± 140 (Fig. 6f; MSWD = 14) Ma. A single zircon analysis that was only ~24% concordant was excluded from the analysis. A discordia generated from a geochronology spot taken from a zircon core and its rim provided an age of 3551 ± 71 Ma. Old, concordant ages come from cores and younger ages come from surrounding zoned rims or cores with abundant fractures (Fig. 7).

The highly discordant grain has a Th/U value of 6.2, while the ratios for the other grains range from 0.22 to 0.82 (Table 2).

IN12050. We measured 12 spots on 12 zircon grains from this sample. Two distinct populations emerge from the data: one with a weighted average age of 3470 ± 69 Ma (Fig. 6g) consisting of concordant zircons, and a younger discordant population with a weighted average age of 2864 ±140 Ma. Habits for the separated zircons range from euhedral to anhedral (Fig. 7). Younger ages come from metamict cores or cores with fractures; Th/U ratios for the older population ranges from 0.53 to 0.071 and ranges from 0.077 to 0.84 for the younger population (Table 2).

4.2.3. Boizard Suite

Two A_{boi} samples were selected for geochronology. One was taken to the east of the upper lobe of the NSB, and one was taken from south of the lower lobe (Fig. 1b).

IN12016. A total of 27 geochronology spots were collected on 22 zircon grains. These analyses yielded an upper intercept age of 3128 ± 170 Ma (MSWD = 37) on a Tera-Wasserburg plot (Fig. 6h). Several old grains with ages up to ca. 3700 Ma were also discovered in this sample set, and 4 analyses were found to plot on a horizontal line with an intercept of 1175 ± 340 Ma (MSWD = 29), suggestive of recent lead loss. A total of 6 grains that plot in a cluster on the concordia gave a weighted average age of 2706 ± 19 Ma. The oldest age obtained in this sample, 3704 ± 13 Ma, comes from a core surrounded by zoned igneous overgrowths (Fig. 7). Other zircons with ages older than 3000 Ma also come from core regions, although some of these appear altered and fractured in electron images. The young, discordant ages come from zircons with highly altered cores that appear either as metamict zones or are filled with fractures and inclusions (Fig. 7). We find that Th/U ratios range from 0.032 to 0.84 in this sample set. Concordant analyses on the

smaller grains typically have either very large or low values, and discordant zircons have Th/U ratios that are highly variable (Table 2).

IN12054. A total of 16 spots on 15 zircons gave an upper intercept age of 3014 ± 170 Ma (Fig. 6i; MSWD = 7.9). A weighted average of the 8 analyses clustered together on the concordia provided an age of 2720 ± 27 Ma. We found that 2 grains in this sample set are concordant, but are significantly older than the population of 2720 Ma zircons. The oldest analysis yields an age of 3431 ± 6 Ma and comes from a core surrounded by a rim that is 2921 ±9 Ma. The other analysis comes from a core that 3175 ± 7 Ma. The grains from the younger but still concordant population have euhedral to anhedral habit (Fig. 7). The Th/U ratios for these grains range from 0.062 to 1.4; the highest values come from the ~2700 Ma grains and the lowest come from the oldest grains (Table 2).

4.2.4. USB Enclaves

Three samples from the USB for which geochemical data were available (*Sec. 4.1.4*) were also selected for geochronology. One of these was taken in the upper lobe, and two samples were taken from the lower lobe of the *Ukalik* outcrops.

IN12017. A total of eight spots on eight grains yielded an upper intercept age of 3598^{+44}_{-37} Ma (Fig. 6j; MSWD = 2) after a single highly discordant grain was removed from the analysis. Several of the discordant grains have textures typical of hydrothermal growth or metamictization (Corfu et al., 2003). The most concordant of these ages, 3653±8 Ma, comes from a core with a thick, zoned overgrowth (Fig. 7). The Th/U ratio of this spot is 0.74, while other zircons have ratios between 0.07 and 0.23 (Table 2).

IN12042. Six analyses on five grains yielded an upper intercept of 3492 ± 190 Ma (Fig. 6k; MSWD = 8). These grains typically have cores surrounded with younger zoned rims (Fig. 7).

Th/U ratios for this sample ranges from 0.35 to 0.62. Concordant analyses typically have larger Th/U ratios than discordant ones (Table 2).

IN12053. A total of 12 analyses were performed on 11 grains. There are three populations in this sample, and all are discordant (Fig. 6l). The youngest, most discordant grains yielded a weighted average age of 2292 ± 120 Ma. Most zircons from this sample are within 25% concordance with a weighted average age of 3362 ± 19 Ma. The oldest population consists of two grains with ages of 3582 ± 9 Ma and 3694 ± 9 Ma. These grains are euheral to subhedral, and the oldest age domains correspond to zircon cores that are surrounded by rims that have spongy textures typical of hydrothermal alteration (Hoskin and Schaltegger, 2003; Fig. 7). Young zircon ages come from rims or metamict cores, and Th/U values for this sample range from 0.042 to 1.7 (Table 2).

4.3. Zircon Trace-element Geochemistry

The lattice strain model for ionic compatibility between the composition of a mineral (e.g. zircon) and a melt of the composition of the host rock (Blundy and Wood, 1994) is now extensively used as a robust means to determine whether a particular mineral age population is native to its host rock (e.g. Manning et al., 2006; Cates and Mojzsis, 2009; Cates et al. *in revisions*). In those rocks with complex multiple zircon age populations, this model can determine the true age of the rock under the reasonable assumption that the original melt and "native" zircons formed in equilibrium. The model takes advantage of the chemical similarities of the trivalent rare earth elements, where the main controlling factor for how easily these ions are incorporated into growing zircon is the predictable change in ionic radius with increasing atomic number (the Lanthanide contraction). It has long been known that HREE are more compatible in zircon than LREE because their ionic radii approach that of Zr (0.84 Å in eight-fold coordination). Thus, the distribution of the REEs in zircon is controlled by the composition

of the melt and REE_{Zr}/REE_{rock} should plot as a perfect parabola for a zircon that crystallized in a melt with the composition of the rock (Blundy and Wood, 1994). A subset of concordant zircons from the Voizel and CTG suites were selected for REE analysis and lattice strain modeling in order to determine the most likely age of emplacement for these two units. Results of the modeling output are presented in Table 3.

4.3.1 Voizel Suite

Seven zircons from the Voizel suite were selected for REE analyses. Of these, three have very good fits with their host-rock compositions. Zircon 4.1 from sample IN12027 is 3530 ± 9 Ma and had the best fit (R^2 = 0.96; Fig. 8a). The core of zircon 4.4 from IN12027, which is 3527 ± 8 Ma, also has a good fit (R^2 = 0.88; Fig. 8a), as does zircon 4.8 from IN12046, which is 3514 ± 3 Ma (R^2 = 0.89; Fig. 8b). Two old zircons analyzed in sample IN12046 (zircons 4.2 and 4.16) have low R^2 values (0.50 and 0.61, respectively; Fig. 8b), however, the geochronology spots that were overlapped had large fractures running through them. Younger zircons of the Voizel have poor fits. Zircon 5.15 from sample IN12046 (2716 ± 5 Ma) has an R^2 value of 0.64 (Fig. 8b), and the rim of zircon 4.4 from sample IN12027 (3317 ± 4) has an R^2 value of 0.76 (Fig. 8a).

4.3.2 Central Tonalite Gneiss

Five zircons from the CTG were selected for REE analysis. The four grains from sample IN12012 all have better fits than the grain from sample IN05001. Grain 12 from IN05001 has an age of 3482±4 Ma and an R^2 value of 0.45 (Fig. 8c). Zircon grain 6.9 (3659±7 Ma) from IN12012 has the poorest fit in that sample, with an R^2 value of 0.79 (Fig. 8c), although like in several of the Voizel sample, the geochronology spot overlaid a fracture in the grain. The other 3 grains are slightly older: zircon 6.5 is 3661 ± 8 Ma and has an R^2 value of 0.94, zircon 6.10 is

3663 ± 5 Ma and has an R^2 value of 0.92, and zircon 6.4 is 3663 ± 6 Ma and has an R^2 value of 0.89 (Fig. 8d)

5. Discussion

5.1. Geochemical and geochronological assignments for the Voizel Suite and Central Tonalitic Gneiss

Although originally considered part of the same suite, new evidence shows that the A_{voi} and CTG belong to separate generations of TTG gneisses in the Inukjuak domain. All the felsic gneisses analyzed here yield multi-element plot patterns that conform with classic continental crust signatures, and with negative Nb and Ti anomalies (Fig. 4; Rudnick, 1995). Both units comprise mostly tonalitic gneisses with about 70 wt.% SiO_2 and moderate concentrations of alkalis ($NaO+CaO+K_2O$ ~ 9.0 wt.%; Table 1). However, the A_{voi} suite rocks appear to be more depleted in REEs (particularly the HREEs) than those from the CTG. Interestingly, the two Voizel suite rocks that plot in the quartz monzonite field as opposed to the tonalite field of Barker (1979; Fig. 3) also have positive Eu anomalies. Gneissic rocks with these types of features (Low REE concentrations, positive Eu anomalies) in metamorphic terrains have been interpreted as likely leucosomes during migmatite formation (Sawyer, 2008; see also Cates et al. *in revisions*).

Although these small geochemical differences could be the result of internal variability, the geochronological differences between these two suites point to separate generations of TTG gneisses for the A_{voi} and CTG. As previously noted (*Sec. 4.2.2*), the A_{voi} suite appears to be ca. 3550 Ma based on upper intercept ages even if it has no individual zircon analyses that provide ages greater than 3538 ± 6 Ma (from sample *IN12046*), and the zircon with the best fit for the lattice strain model is 3530 Ma (99% concordant).

In contrast to the A_{voi} samples, the CTG sample *IN12012* has abundant zircons with ages up to 3663 ± 5 Ma, and the zircon with the best fit for the lattice strain model is 3661 ± 8 Ma. The ca. 3660 Ma zircons from CTG sample *IN12012* are dominated by oscillatory zoned cores with thin rim overgrowths. The ca. 3660 Ma cores are consistent with igneous growth and we interpret this to be the maximum age of the CTG. Zircons from another CTG sample *IN05001*, are only ca. 3450 Ma. These zircons, however, show poor fits with the lattice strain model and are unlikely to represent igneous growth in a melt with the host-rock composition. Thus, we can conclude that the age of the CTG as determined by the upper intercept of the discordia on a Tera-Wasserburg plot is 3652 ± 14 Ma. This age is about 100 Myr older than the new assigned age of the A_{voi} suite. David et al. (2009) presented geochronological data for a single mylonitized sample from the northwest of the margin of the NSB that was also ca. 3660 Ma. We note that this age is statistically indistinguishable from the ages presented herein for the CTG, and speculate that this rock is most likely related to the CTG rather than to the more widely distributed A_{voi} suite.

5.2. Geochemical and geochronological assignments for the Boizard Suite

The A_{boi} suite is geochemically distinct from the other granitoid gneisses described for the Inukjuak domain. It is a granite and lacks the strong tectonic fabric (foliation) observed in the A_{voi} and CTG outcrops. Zircons from the A_{boi} suite show abundant ca. 2700 Ma ages, with some degree of inheritance. Older inherited zircon ages all occur in rounded zircon cores, some of which are surrounded by what appear to be para-igneous rims with strong oscillatory zoning of unknown ages. The inherited cores of the A_{boi} suite zircons include ages previously seen in the NSB (see Cates et al., 2013). This suggests that the A_{boi} granites were extensively contaminated by zircons from the supracrustals during emplacement.

5.3. USB Enclaves

The three TTG gneisses sampled for this study were selected because they were mapped to cross-cut USB amphibolites are significantly younger those found in the ca. 3800 Ma Nuvvuagittuq outcrops further to the west. Zircons from the oldest Ukalik supracrustal enclave sample yielded an upper intercept of only 3598^{+44}_{-37}, although the oldest and still highly concordant individual grain (5% reversely discordant) is 3653±8 Ma (Table 2). These ages might be interpreted as evidence that modification and dismemberment of the USB was contemporaneous with the emplacement of the CTG. The gneiss which preserves the oldest age in this sample set is tonalitic (Fig. 3) with less than 200 ppm Zr (Table 1), thus making inheritance an unlikely source for the oldest grains. The two other supracrustal gneiss samples are granodioritic (Fig. 3). One of these (*IN12053*) has a zircon population at 3362 ± 19 Ma (weighted average of 4 analyses), but they are only within about 15% of concordia. It also has two older grains at 3694±9 Ma and 3582±9 Ma, but these grains are also discordant (~30%). All of these analyses come from zircon cores with oscillatory zoning and thus an absolute determination of the age of the unit cannot be established. However, the low Zr content of this sample (111 ppm; Table 1) coupled with the field relationships, where this sample is part of an enclave contained within the A_{voi}, argues against inheritance. The age of this particular unit is perhaps best represented by the oldest analyses. Many of the younger ages of the zircons within this sample are about 2700 Ma, indicating that the event that disturbed these zircons was related to the emplacement of the A_{boi} suite. This is unsurprising, as sample *IN12053* is located on the eastern edge of the lower lobe of the A_{voi} suite, close to the contact with the Boizard. This age is not seen in the other enclave samples thus far analyzed. Only five zircons were analyzed from sample *IN12042*, the oldest of which is 3529 ± 8 Ma.

6. Conclusions

Diverse granite-granitoid gneisses of the Inukjuak domain which host supracrustal enclaves, including some of the oldest supracrustal rocks thus far recognized at the Nuvvuagittuq locality, were emplaced over multiple generations over a protracted history. These dated intrusive events, distributed as they were over space and time, disrupted and metamorphosed the various supracrustal enclaves of the *Innucsuac Complex* and are recorded as episodes of metamorphic zircon growth within the enclaves (Cates and Mojzsis, 2007, Cates et al., 2013). Results from detailed U-Pb zircon geochronology of samples collected in the vicinity of both the Nuvvuagittuq and Ukalik supracrustal belts reveal multiple generations of zircon growth spanning from ca. 3800 to 2700 Ma. Lattice strain partition modeling differentiates between these different age populations based on compositional parameters, and reveals the most likely crystallization age for each unit. Based on this combined approach, the age of the CTG can be resolved to ca. 3650 Ma. The previously undated Voizel suite is some 100 Myr younger than this, with a maximum age of about 3550 Ma. The Boizard suite, which we can be confidently assigned a ca. 2700 Ma age, experienced widespread contamination during its emplacement and carries inherited zircons from all older suites in the terrane including those from the NSB. Disruption and partial structural dismemberment of the Ukalik supracrustal belt may be contemporaneous to the timing of the formation of the CTG. This age relationship provides a tentative petrogenetic link to the neighboring ca. 3750-3780 Ma Nuvvuagittuq supracrustal belt (Cates and Mojzsis, 2007; Cates et al., 2013).

References

Anders E., Grevesse N., 1989. Abundances of the elements- meteoric and solar. Geochimica et Cosmochimica Acta 53, 197-214.

Barker, F., 1979. Trondhjemite: definition, environment and hypothesis of origin. In: F. Barker (Ed.), Trondhjemites, Dacites and Related Rocks. Elsevier, Amsterdam, 1–12.

Black L.P., Kamo, S.L., Williams I.S., Mundil R., Davis D.W., Korsch R.J., Foundoulis C., 2003. The application of SHRIMP to Phanerozoic geochronology; a critical appraisal of four zircon standards. Chemical Geology 200, 171–188

Blundy J., Wood B., 1994. Prediction of crystal-melt partition coefficients from elastic moduli. Nature 372, 452-454.

Cates N.L., Mojzsis S.J., 2007. Pre-3750 Ma supracrustal rocks from the Nuvvuagittuq supracrustal belt, northern Québec. Earth and Planetary Science Letters 255, 9–21

Cates N.L., Mojzsis S.J., 2009. Metamorphic zircon, trace elements and Neoarchean metamorphism in the ca. 3.75 Ga Nuvvuagittuq supracrustal belt, Québec (Canada). Chemical Geology 261, 98–113

Cates N.L., Ziegler K., Schmitt A.K., Mojzsis S.J., 2013. Reduced, reused and recycled: Detrital zircons define a maximum age for the Eoarchean (ca. 3750-3780 Ma) Nuvvuagittuq Supracrustal Belt, Québec (Canada). Earth and Planetary Science Letters 362, 283-293.

Cates N.L., Mojzsis S.J., Caro, G., Trail D., Abramov O., Guitreau M., Hopkins M.D., Blichert-Toft J., Bleeker W. (in revision). Geochimica et Cosmochimica Acta.

Corfu F., Hanchar J.M., Hoskin P.W.O., Kinny P., 2003. Atlas of zircon textures. Reviews in Mineralogy and Geochemistry. 53, 469–500.

David, J., Stevenson, R.K., Nadeau, P., Godin, L., 2002. La séquence supracrustale de Porpoise Cove, région d'Inukjuak: un exemple unique de croûte paléo-archéenne (ca. 3.8 Ga) dans la Province du Supérieur. In: L'exploration minérale au Québec, notre savoir, vos découvertes. Ministère des Ressources Naturelles, Québec. DV 2002, 17.

David J., Godin L., Stevenson R., O'Neil J., Francis D., 2009. U–Pb ages (3·8–2·7 Ga) and Nd isotope data from the newly identified Eoarchean Nuvvuagittuq supracrustal belt, Superior Craton, Canada. Geological Society of America Bulletin 121, 150-163.

de Witt M., Ashwall L.D., 1997. Greenstone belts. Oxford Monographs on Geology and Geophysics 35.

Frank E.A., Maier W.D., Mojzsis S.J. (in preparation). Platinum group abundance trends in Eoarchean komatiite protoliths. Chemical Geology.

Hoskin P.W.O., Schaltegger U., 2003. The composition of zircon and igneous metamorphic petrogenesis. Reviews in Mineralogy and Geochemistry 53, 27–62

Ludwig, K.R., 2003. User's Manual for Isoplot/Ex: A Geochronological Toolkit for Microsoft Excel, Berkley Geochronological Center Special Publication.

Manning C.E., Mojzsis S.J., Harrison, T.M., 2006. Geology, age and origin of supracrustal rocks, Akilia, Greenland. Am. J. Sci. 306, 303-366.

McDonough W.F., 1992. Composition of the primitive mantle, depleted mantle and other mantle reservoirs. International Geological Congress. 29, A175

O'Neil J., Maurice C., Stevenson R.K., Larocque J., Cloquet C., David J., Francis D., 2007. The geology of the 3·8 Ga Nuvvuagittuk (Porpoise Cove) Greenstone Belt, northern Superior Province, Canada. In: Kranendonk M.J., Smithies R.H., Bennett V.C., editors. Earth's Oldest Rocks. Elsevier, Amsterdam, pp. 219-250.

O'Neil J., Carlson R.W., Francis D., Stevenson R.K., 2008. Neodymium-142 evidence for Hadean mafic crust. Science 321, 1828-1831.

O'Neil J., Francis D., Paquette J., Carlson R.W., 2012. Formation age and metamorphic history of the Nuvvuagittuq Greenstone Belt. Precambrian Research 220, 23-44

Paces J.B., Miller J.D., 1993. Precise U-Pb ages of Duluth Complex and related mafic intrusions, northeastern Minnesota - Geochronological insights to physical, petrogenic, paleomagnetic, and tectonomagmatic processes associated with the 1.1 Ga Midcontinent Rift system. Journal of Geophysical Research, Solid Earth 98, 13997-14013.

Roth A.S.G., Bourdon B., Mojzsis S.J., Touboul M., Sprung P. Guitreau M. Blichert-Toft J., 2013. Inherited ^{142}Nd anomalies in Eoarchean protoliths. Earth and Planetary Science Letters 361, 50-57.

Rudnick R.L., Fountain D.M., 1995. Nature and composition of the continental crust: A lower crustal perspective. Reviews of Geophysics 33, 267-310

Sawyer E.W., 2008. Atlas of Migmatites. The Canadian Mineralogist, Special Publication 9. NRC Research Press, Ottawa, 371

Schmitt A.K., Vazquez J.A., 2006. Alteration and remelting of nascent oceanic crust during continental rupture: Evidence from zircon geochemistry of rhyolites and xenoliths from the Salton Trough, California. Earth and Planetary Science Letters 252, 260-274

Schuhmacher M., de Chambost E., McKeegan K.D., Harrison T.M., Migeon H., 1994. Dating of zircon with the CAMECA IMS 1270. In: Benninghoven A., Nihei Y., Shimizu R., Werner H.W.

(Eds.), Secondary Ion Mass Spectrometry SIMS IX. John Wiley & Sons, New York, pp. 912–922.

Simard M., Parent M., David J., Sharma K.N.M., 2003. Géologie de la région de la rivière Innuksuac (34K et 34L). Ministère des Ressources naturelles, RG, Québec, 2002–10.

Stevenson R., Bizzarro M., 2005. Hf and Nd isotope evolution of lithologies from the 3.8 Ga Nuvvuagittuq Sequence, northern Superior Province, Canada. Geochimica et Cosmochimica Acta 69, A391

Watson E.B., Harrison T.M., 1983. Zircon saturation revisited: temperature and composition effects in a variety of crustal magma types. Earth and Planetary Science Letters 64, 295-304

Figures

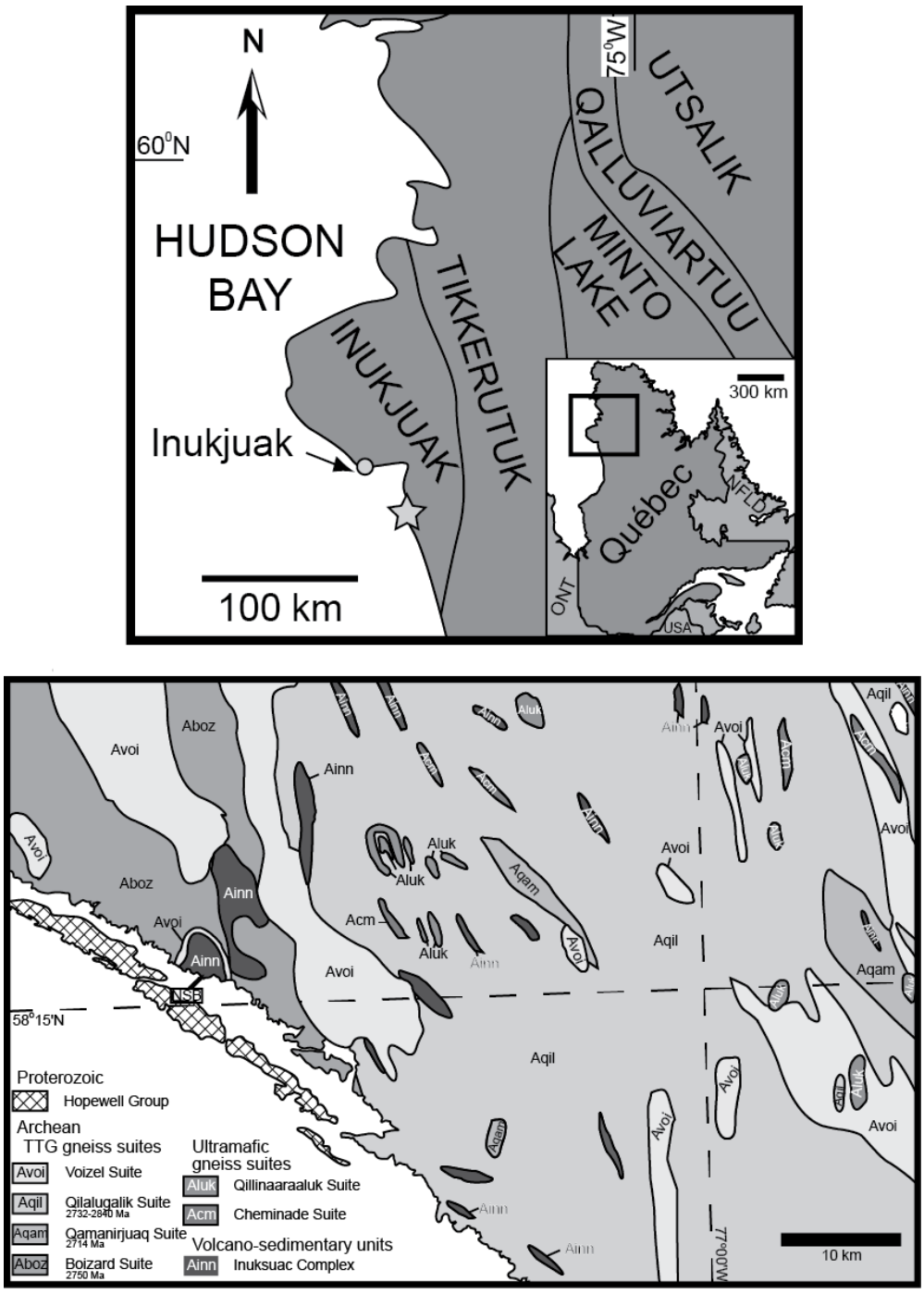

Figure 1a. Simplified maps of the regional geology. Upper panel shows the general division of the northwestern portion of the Hudson Bay Terrain into domains. The inset shows the location on a geographic map of Eastern Canada. The location of the field area is marked by a star. Lower panel shows the local regional geology and geochronology, with the Nuvvuagittuq supracrustal belt labeled NSB. Maps from Cates and Mojzsis (2007), after Simard et al. (2003).

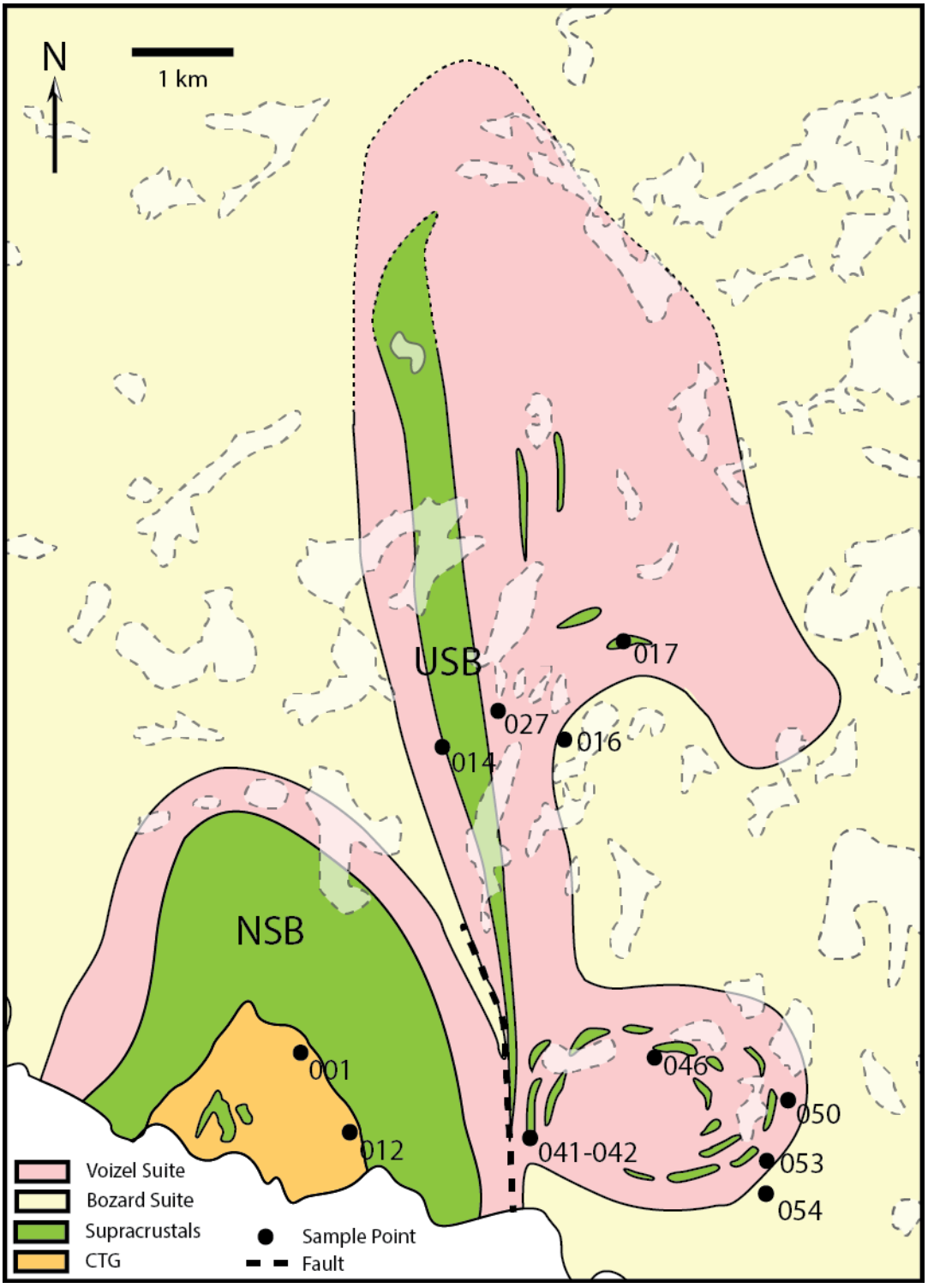

Figure 1b. Geologic map of the NSB and USB with surrounding suites. sample locations labeled with IN12 or IN05 prefix omitted for clarity.

Figure 2a. Field photos of the CTG. Upper panel is the location of sample IN05001. Field of view at bottom of image is approximately 2 m. Lower panel is the location of sample IN12012. Hammer for scale.

Figure 2b. Field photos of the Voizel suite. Both images are the location of sample IN12014. Person for scale in upper panel. Field of view at bottom of lower panel is approximately 2 m.

Figure 2b. Field photos of the Voizel suite. Upper panel is the location of sample IN12027. Hammer for scale. Lower panel is the location of sample IN12041. Hammer for scale.

Figure 2b. Field photos of the Voizel suite. Panel is the location of sample IN12046. Field of view at bottom of image is approximately 2 m.

Figure 2b. Field photos of the Voizel suite. Both panels are the location of sample IN12050. Hammers for scale.

Figure 2c. Field photos of the Boizard suite. Panel is the location of sample IN12016. Knife for scale.

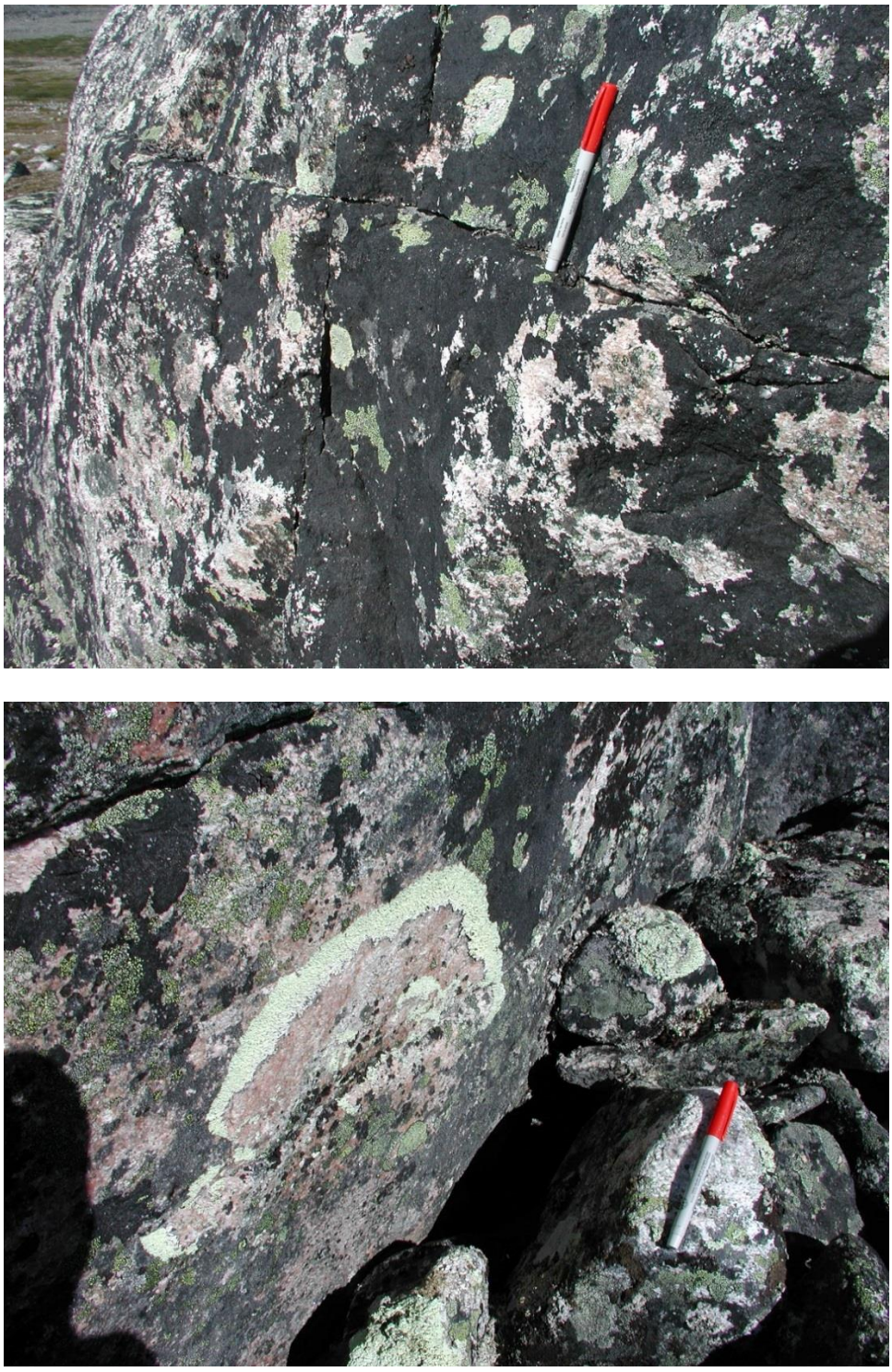

Figure 2c. Field photos of the Boizard suite. Both panels are the location of sample IN12054. Pens for scale.

Figure 2d. Field photos of USB enclaves. Upper panel is the location of sample IN12042 (white). Sledgehammer for scale. Lower panel is the location of sample IN12053. Clipboard and hammer for scale.

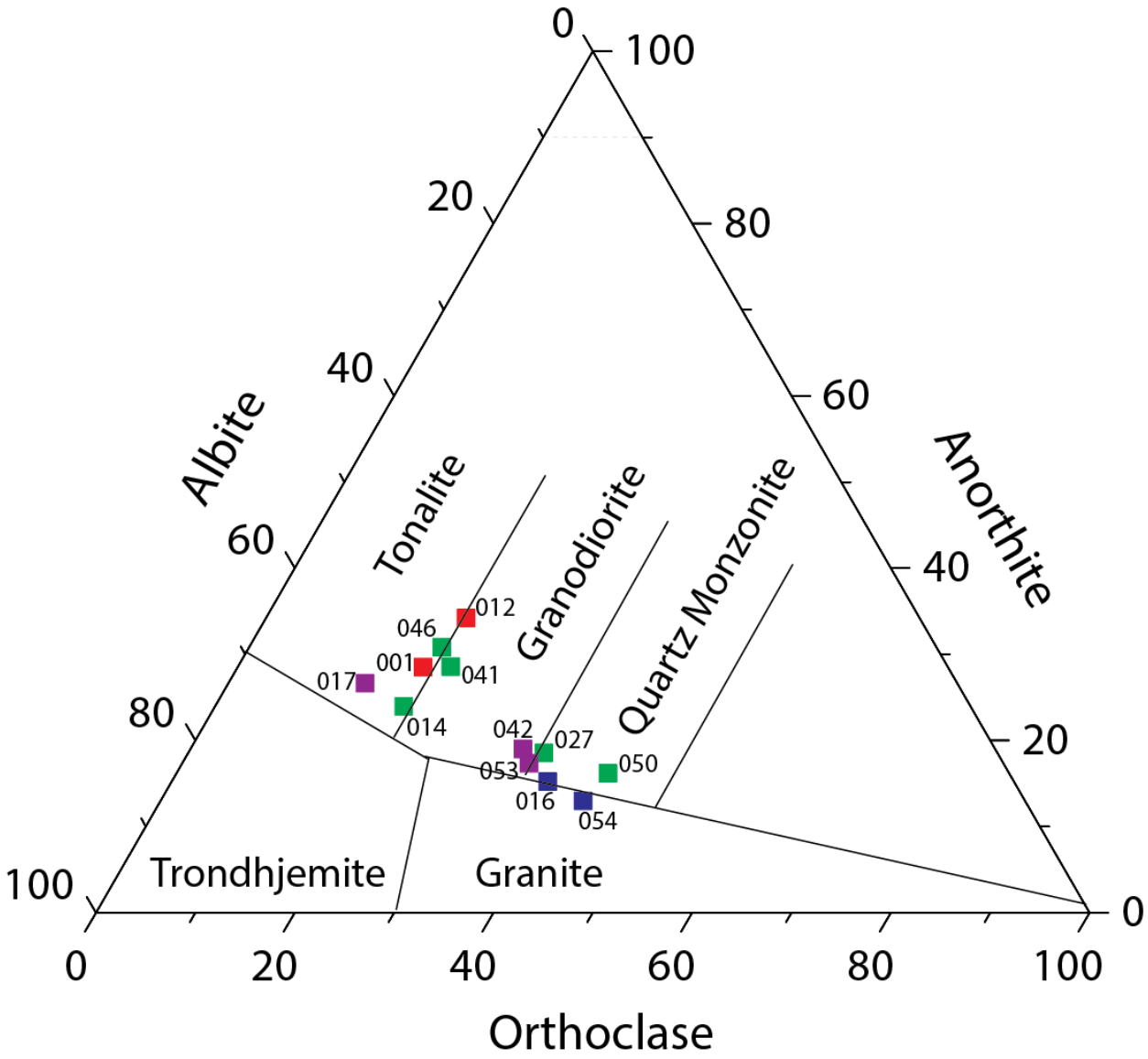

Figure 3. Classification of samples based on normative An-Ab-Or composition. Fields from Barker (1979); CTG = red, Voizel = green, Boizard = blue, USB enclaves = purple. Individual analyses labeled with IN12 or IN05 prefixes omitted for clarity.

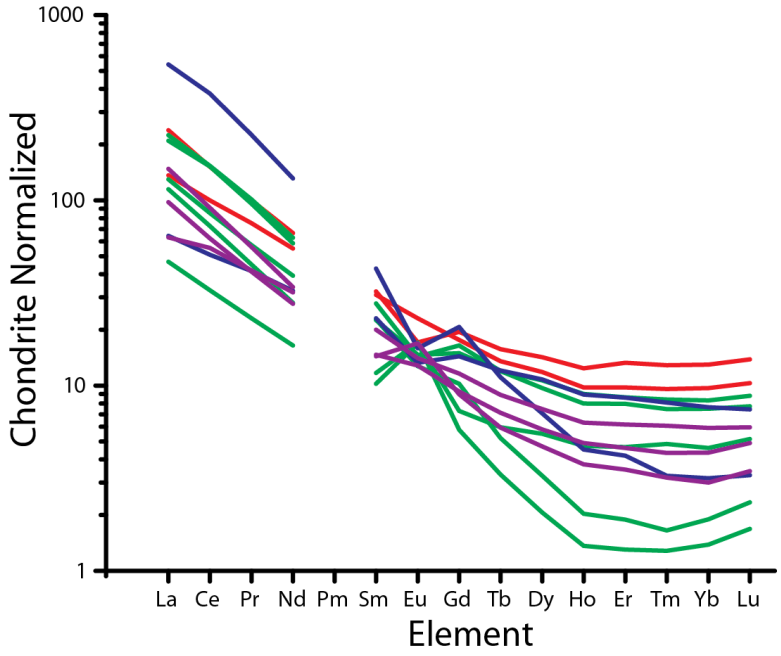

Figure 4. Chondrite normalized (Anders and Grevesse, 1989) REE plot; CTG = red, Voizel = green, Boizard = blue, USB enclaves = purple.

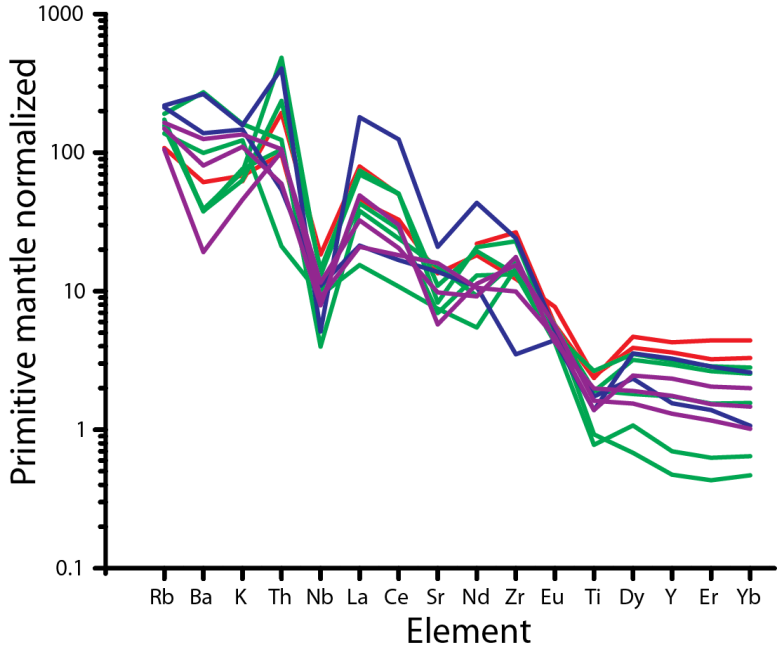

Figure 5. Primitive mantle normalized (McDonough, 1992) multi-element plot; CTG = red, Voizel = green, Boizard = blue, USB enclaves = purple.

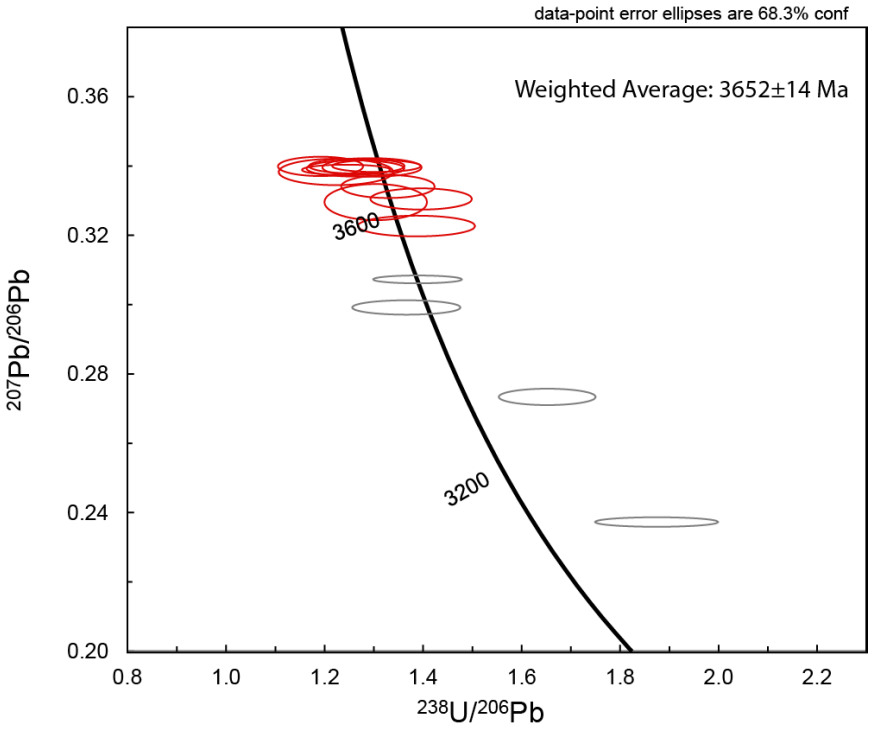

Figure 6a. Tera-Wasserburg concordia plot of U-Pb zircon analyses from sample IN12012. Gray ellipses were not included in weighted average age calculation.

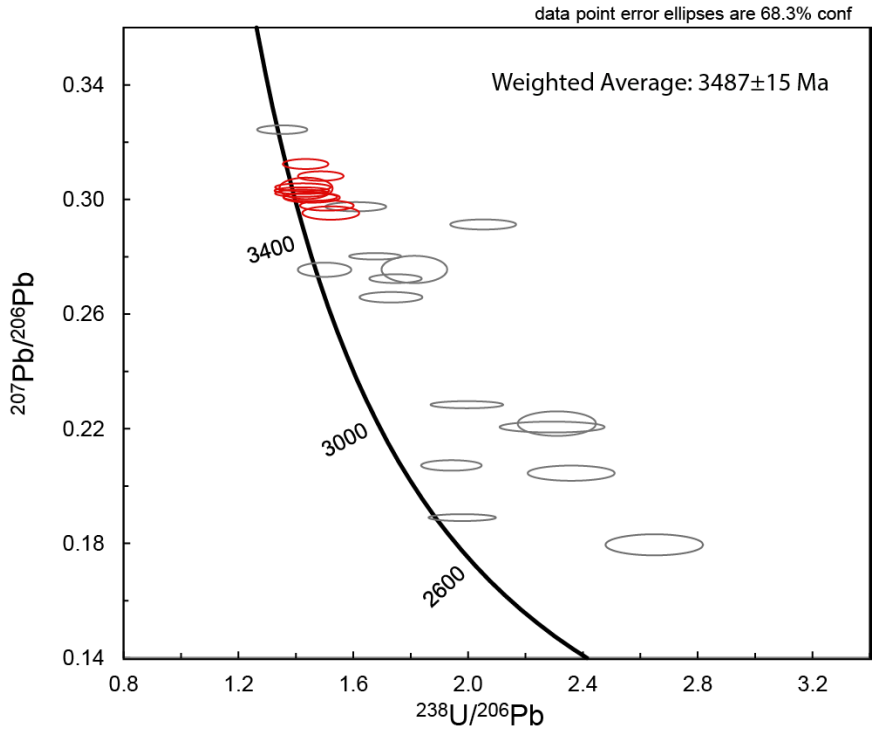

Figure 6b. Tera-Wasserburg concordia plot of U-Pb zircon analyses from sample IN05001. Gray ellipses were not included in weighted average age calculation.

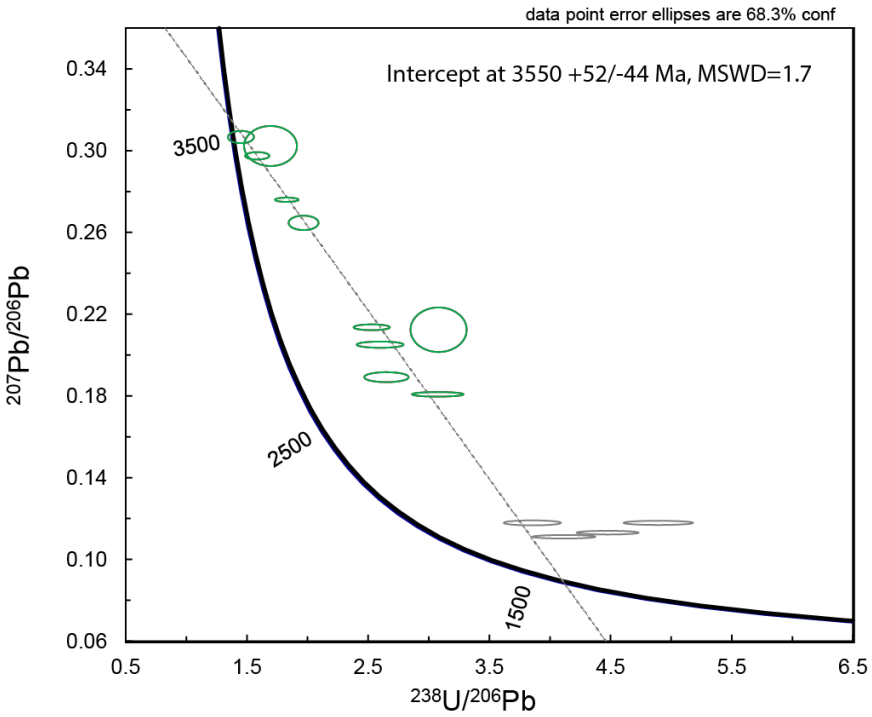

Figure 6c. Tera-Wasserburg concordia plot of U-Pb zircon analyses from sample IN12014. Gray ellipses were not included in discordia age calculation.

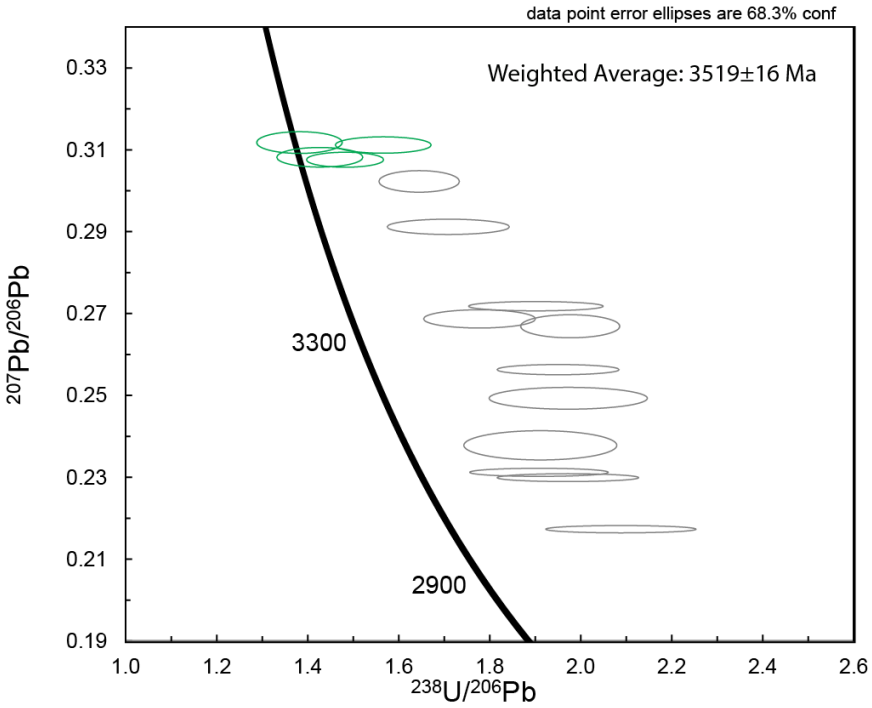

Figure 6d. Tera-Wasserburg concordia plot of U-Pb zircon analyses from sample IN12027. Gray ellipses were not included in weighted average age calculation.

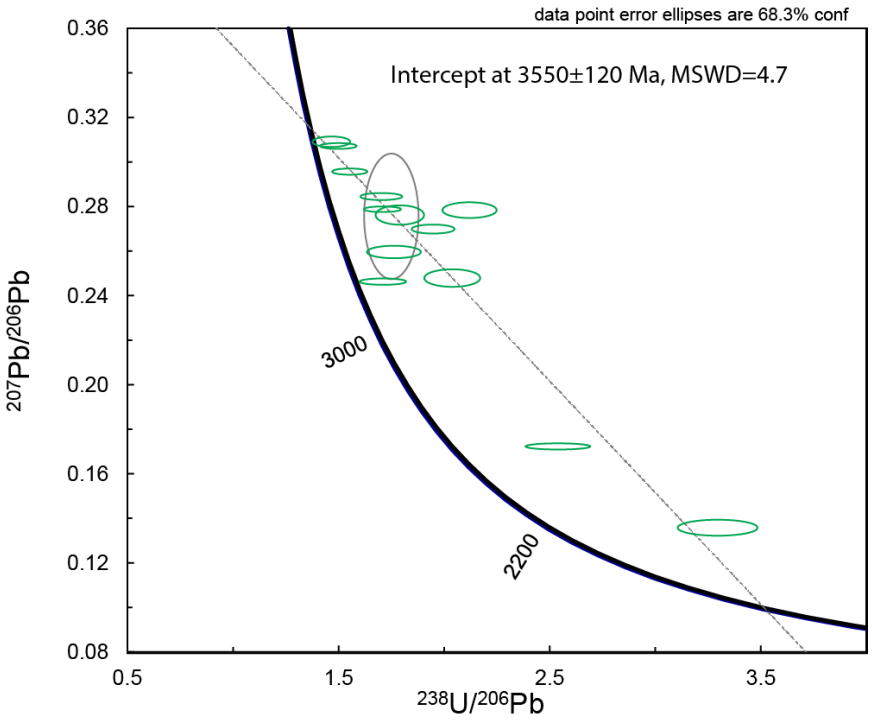

Figure 6e. Tera-Wasserburg concordia plot of U-Pb zircon analyses from sample IN12041. Gray ellipse was not included in discordia age calculation.

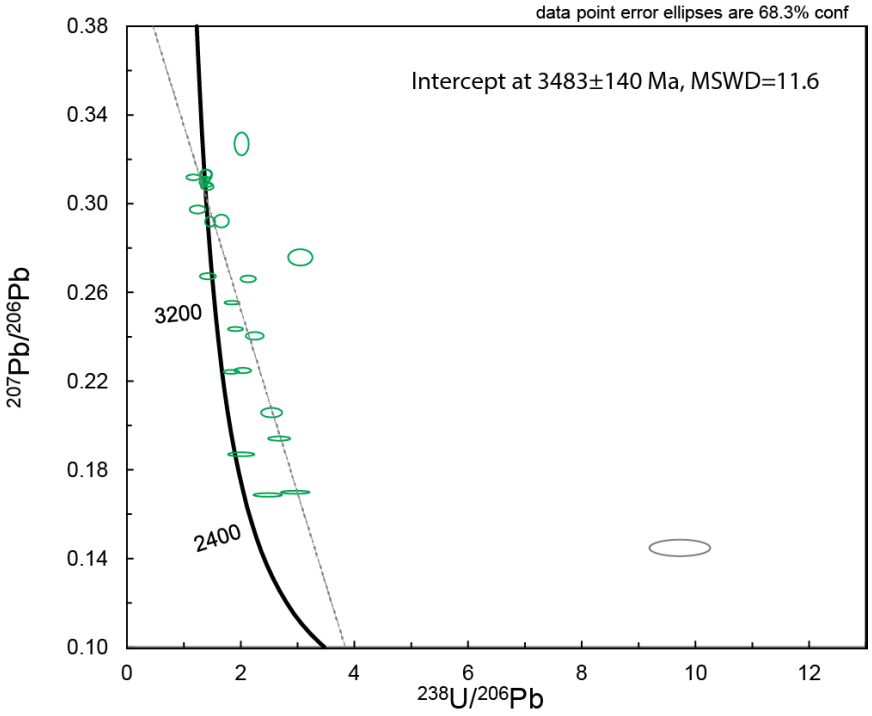

Figure 6f. Tera-Wasserburg concordia plot of U-Pb zircon analyses from sample IN12046. Gray ellipse was not included in discordia age calculation.

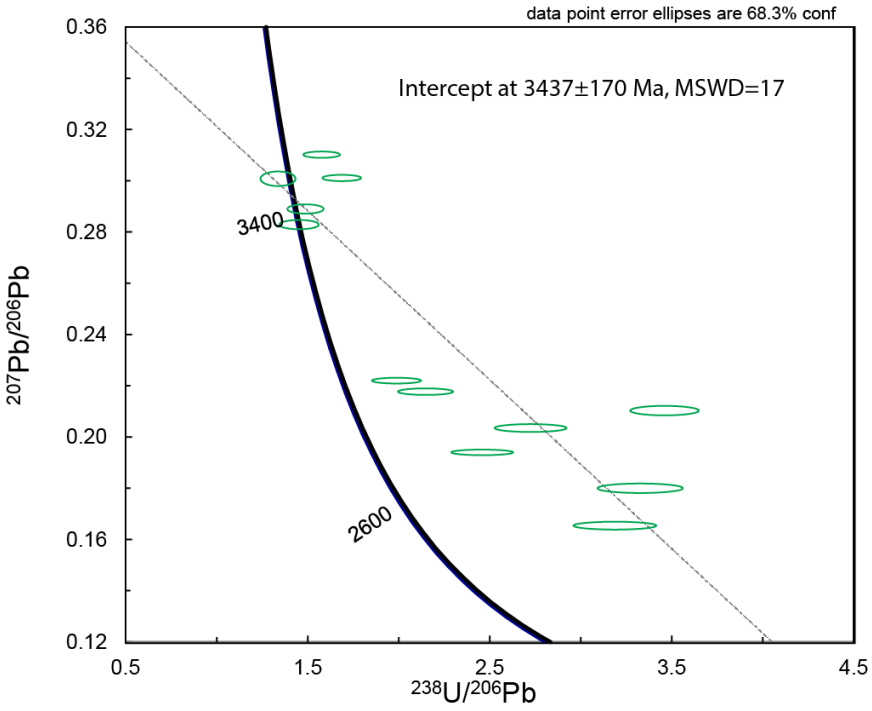

Figure 6g. Tera-Wasserburg concordia plot of U-Pb zircon analyses from sample IN12050.

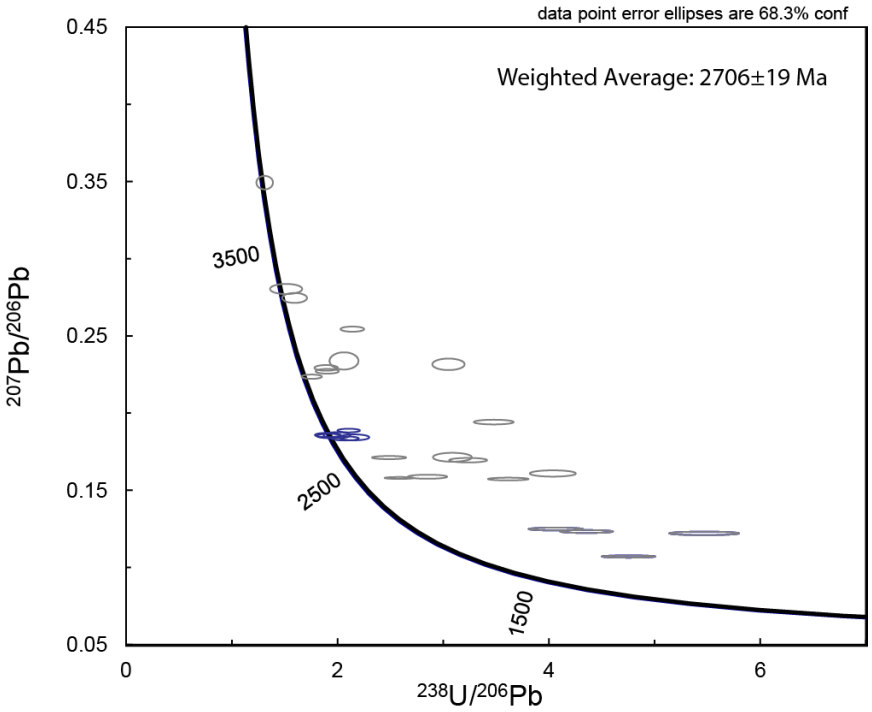

Figure 6h. Tera-Wasserburg concordia plot of U-Pb zircon analyses from sample IN12016. Gray ellipses were not included in weighted average age calculation.

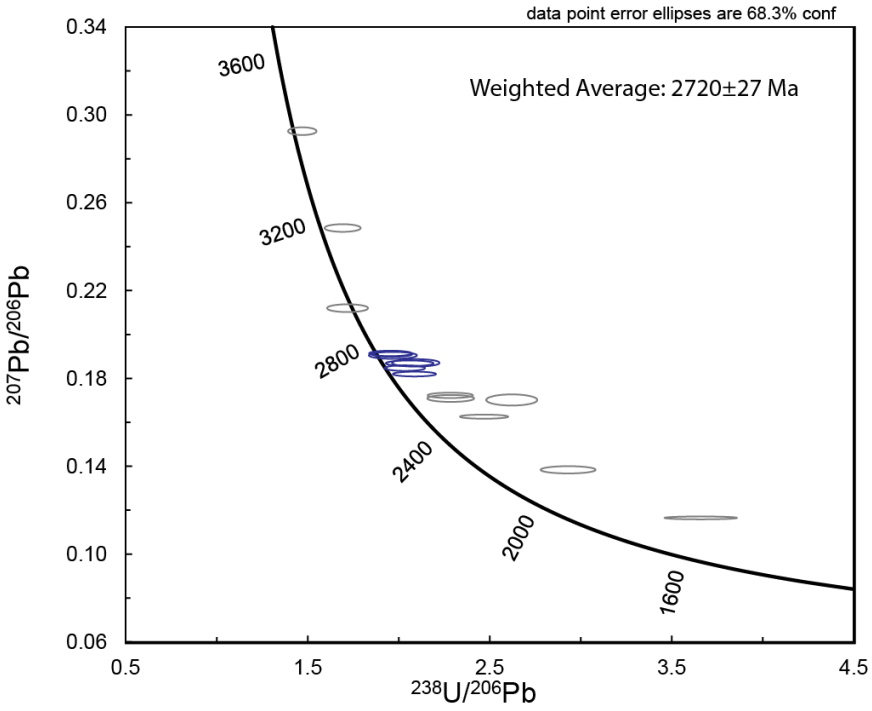

Figure 6i. Tera-Wasserburg concordia plot of U-Pb zircon analyses from sample IN12054. Gray ellipses were not included in weighted average age calculation.

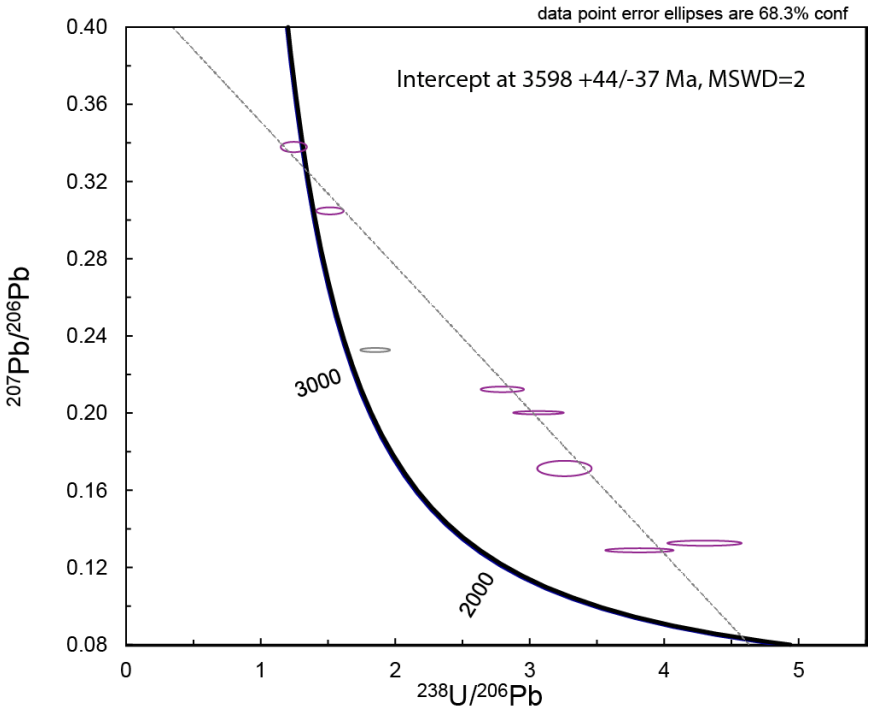

Figure 6j. Tera-Wasserburg concordia plot of U-Pb zircon analyses from sample IN12017. Gray ellipse was not included in discordia age calculation.

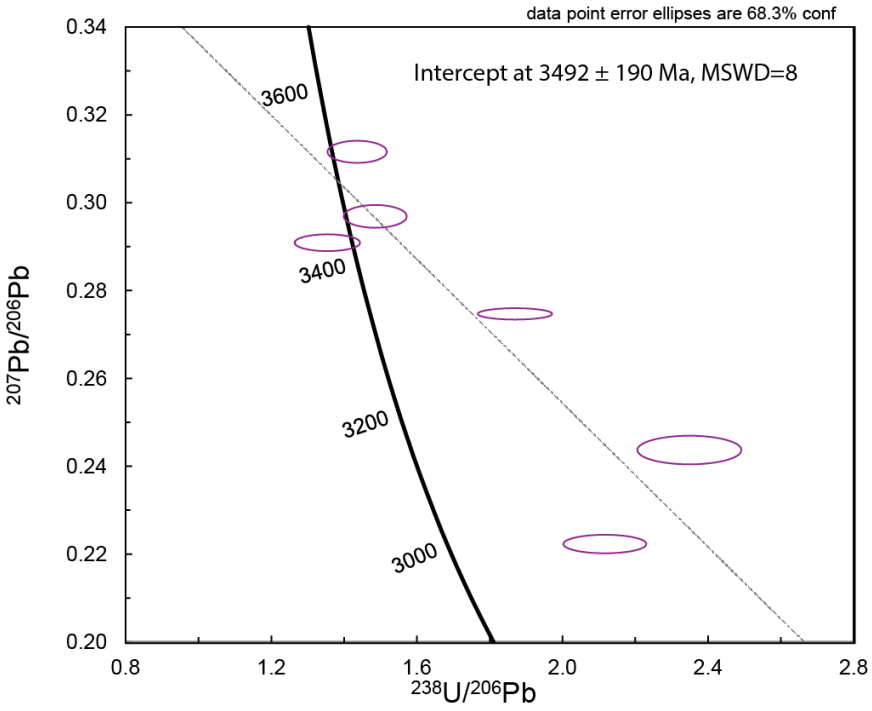

Figure 6k. Tera-Wasserburg concordia plot of U-Pb zircon analyses from sample IN12042.

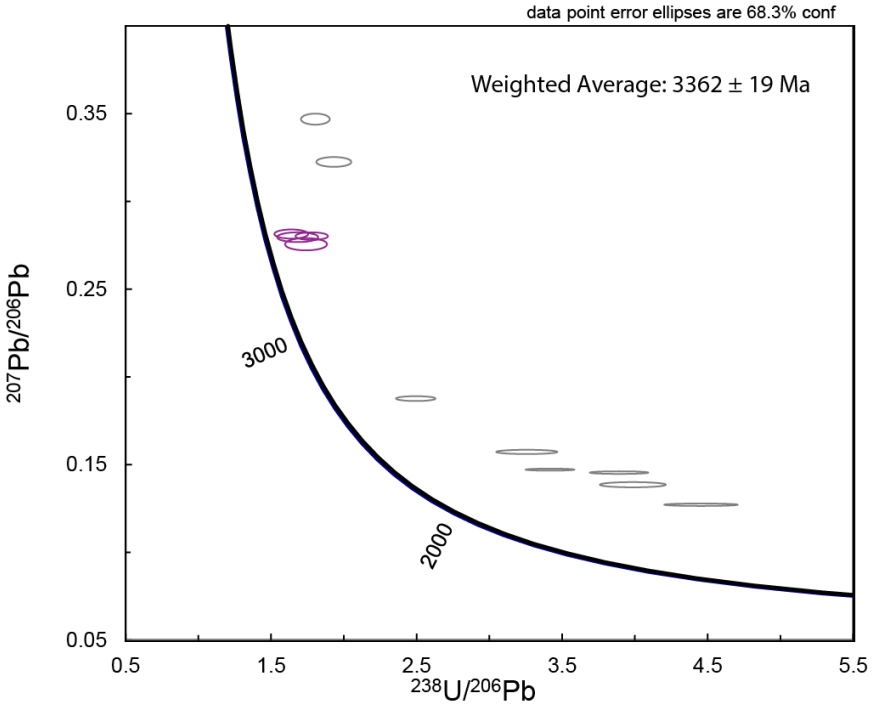

Figure 6l. Tera-Wasserburg concordia plot of U-Pb zircon analyses from sample IN12053. Gray ellipses were not included in weighted average age calculation.

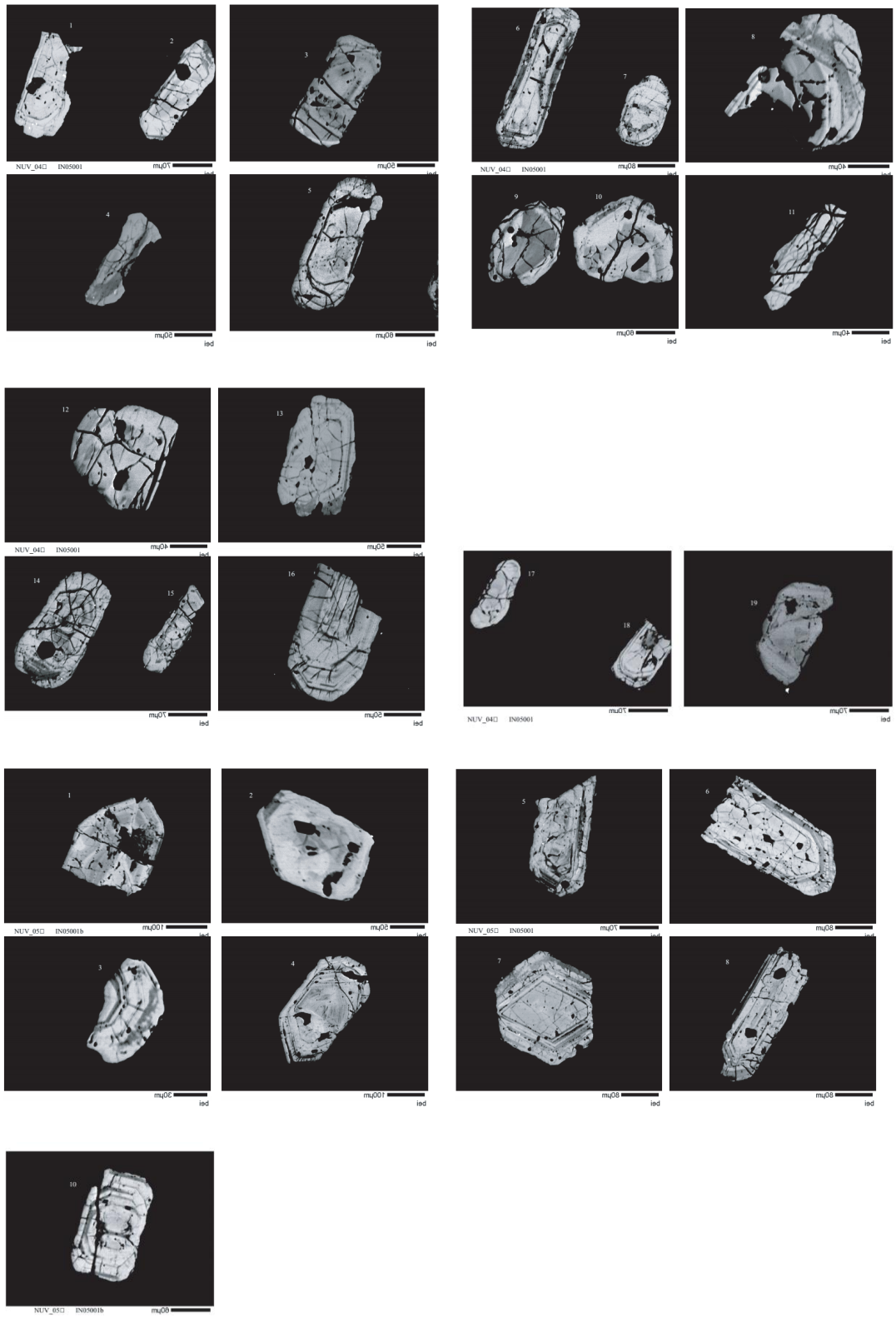

Figure 7. Backscatter electron images of zircon grains used in geochronological and trace-element analysis (above: IN05001).

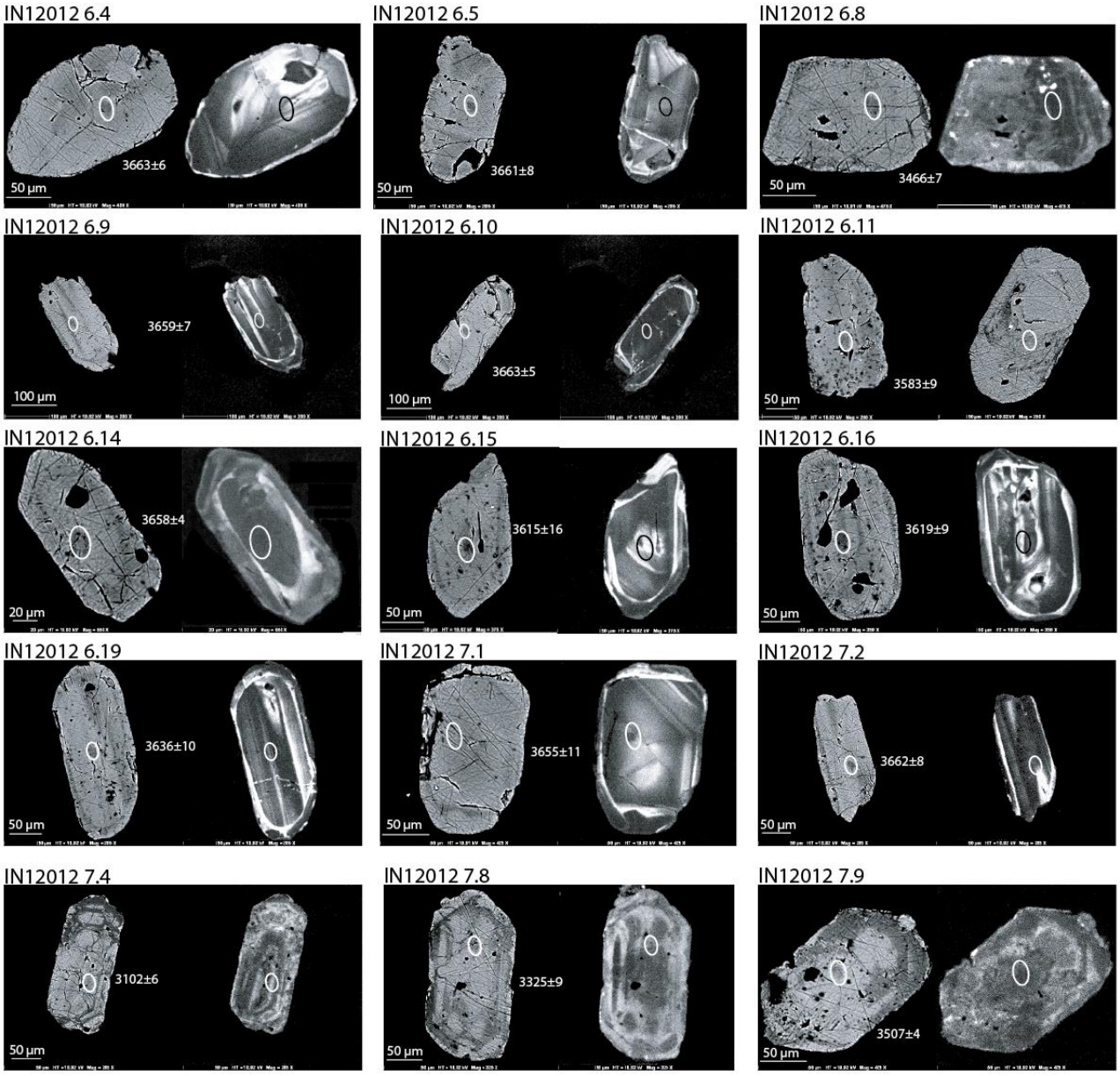

Figure 7. Backscatter electron and cathodoluminescence pared images of zircon grains used in geochronological and trace-element analysis (above: IN12012).

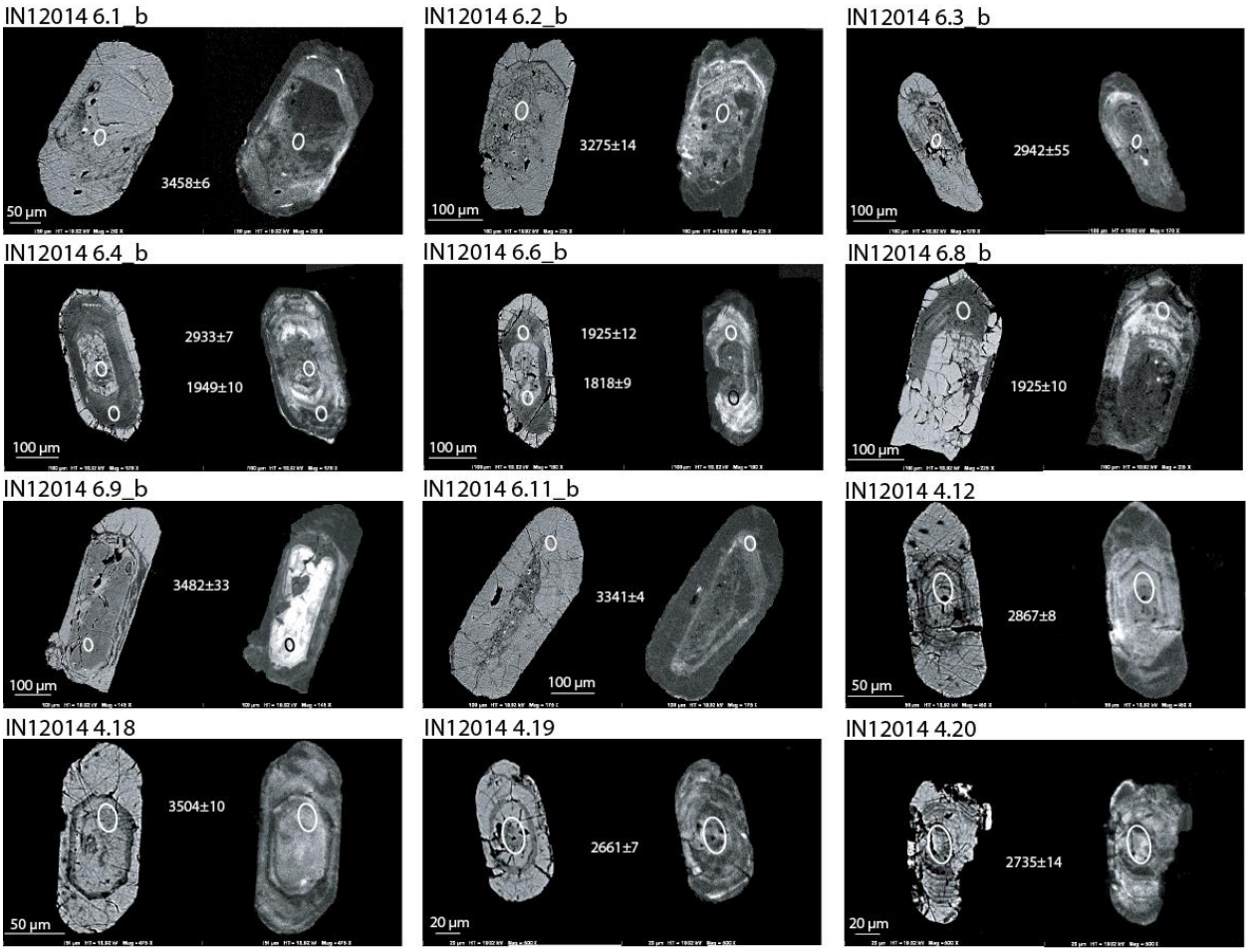

Figure 7. Backscatter electron and cathodoluminescence pared images of zircon grains used in geochronological and trace-element analysis (above: IN12014).

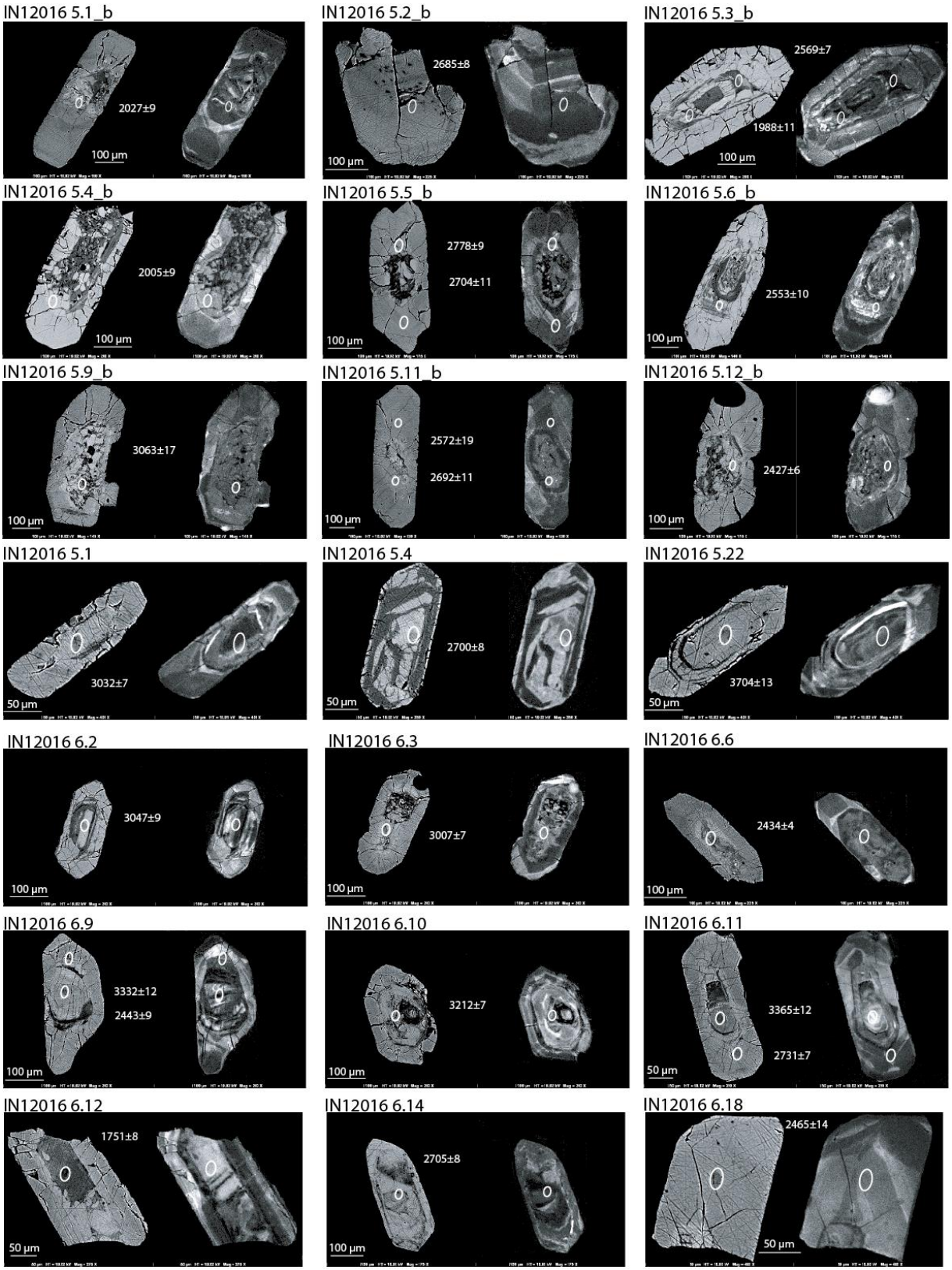

Figure 7. Backscatter electron and cathodoluminescence pared images of zircon grains used in geochronological and trace-element analysis (above: IN12016).

IN12016 6.19

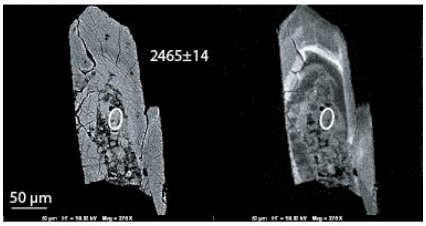

Figure 7. Backscatter electron and cathodoluminescence pared images of zircon grains used in geochronological and trace-element analysis (above: IN12016 cont.).

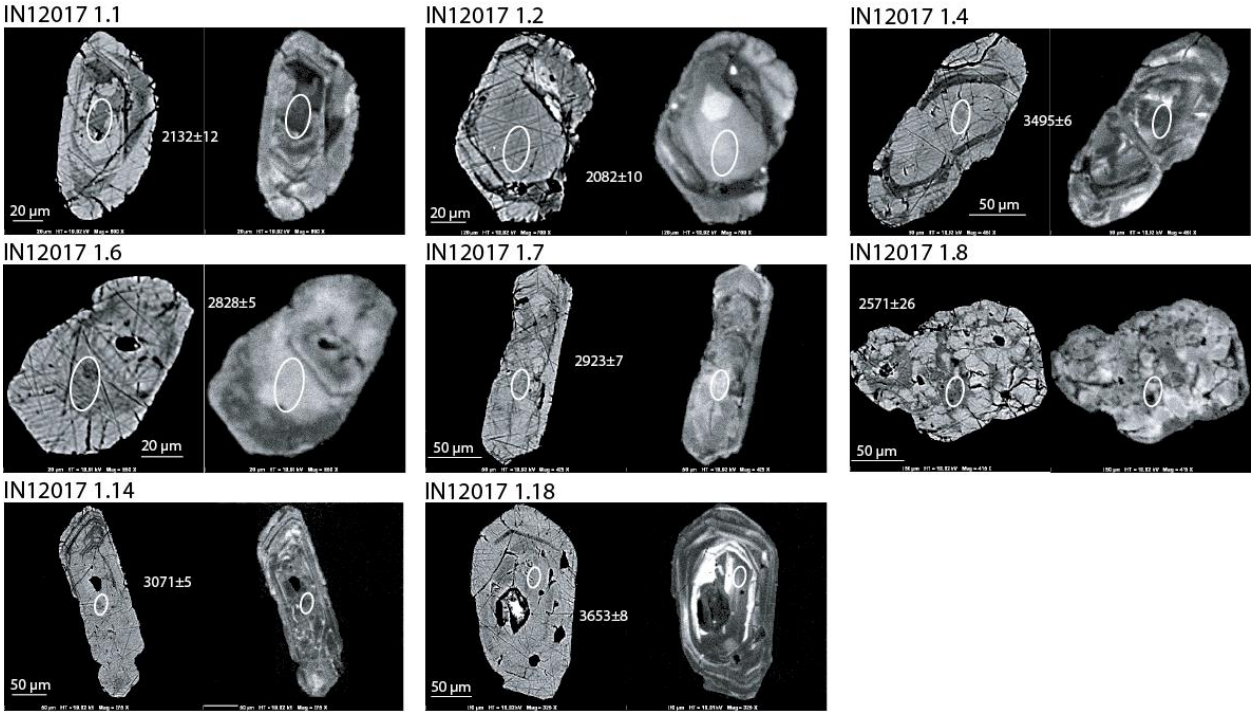

Figure 7. Backscatter electron and cathodoluminescence pared images of zircon grains used in geochronological and trace-element analysis (above: IN12017).

Figure 7. Backscatter electron and cathodoluminescence pared images of zircon grains used in geochronological and trace-element analysis (above: IN12027).

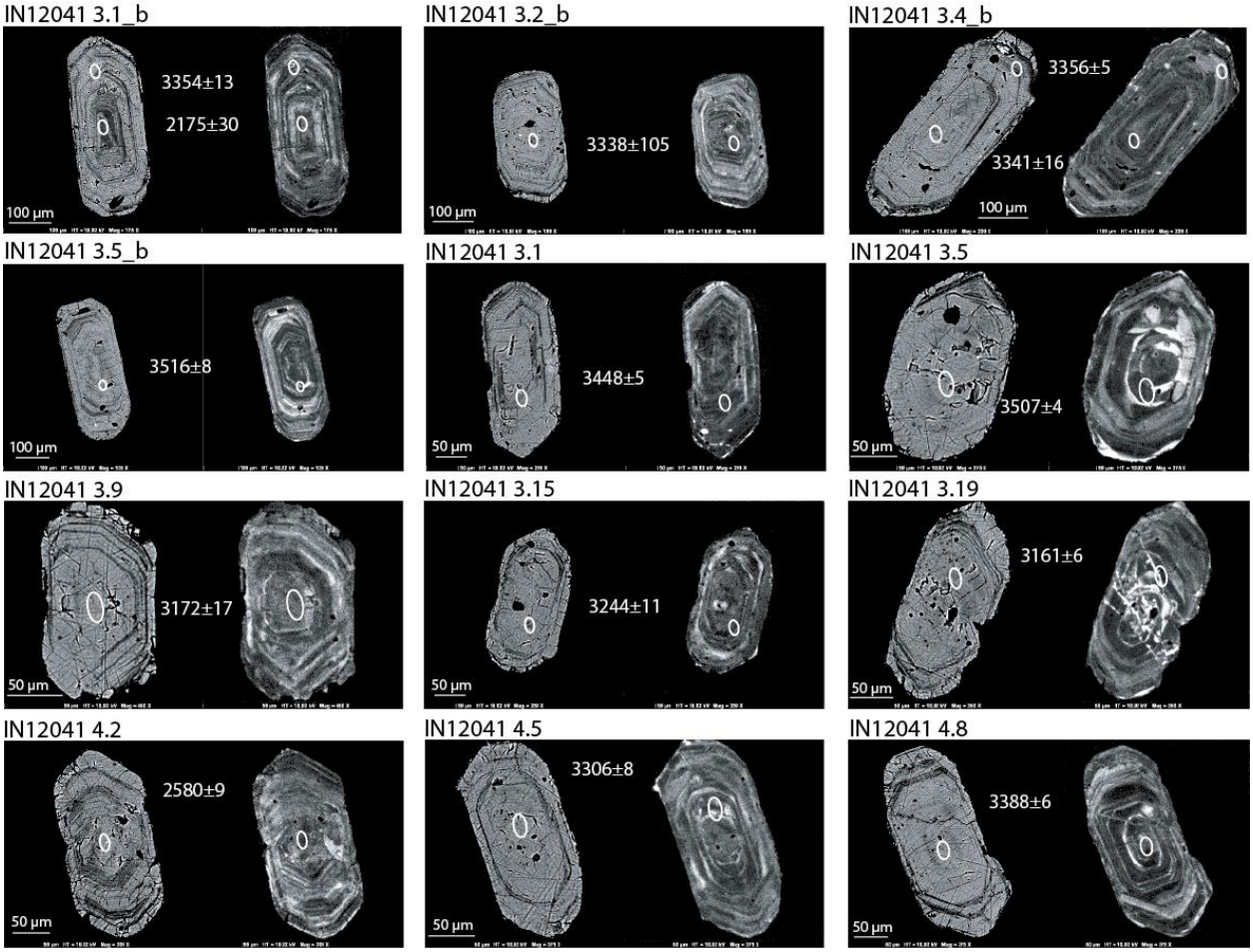

Figure 7. Backscatter electron and cathodoluminescence pared images of zircon grains used in geochronological and trace-element analysis (above: IN12041).

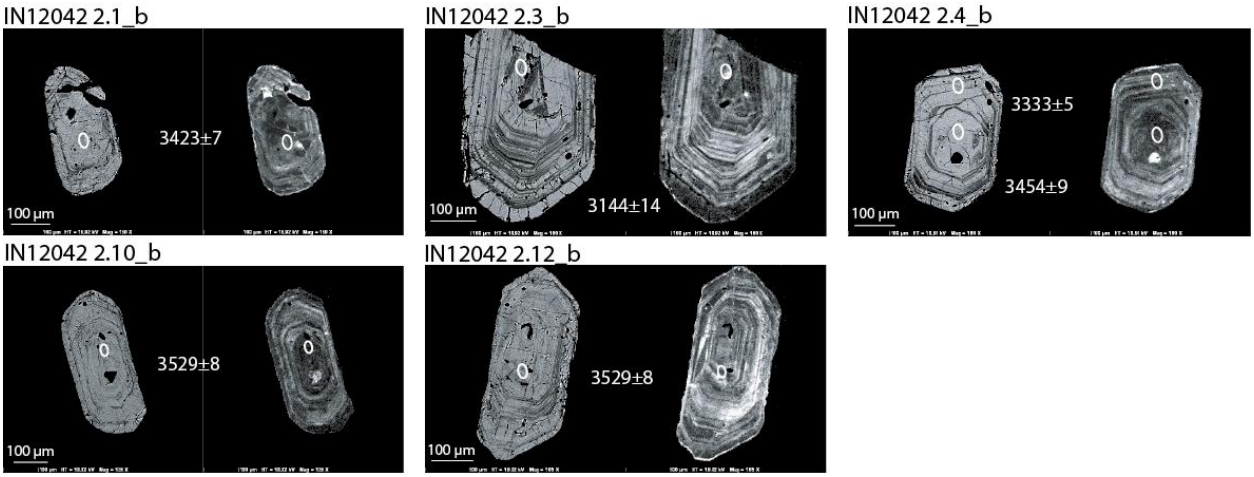

Figure 7. Backscatter electron and cathodoluminescence pared images of zircon grains used in geochronological and trace-element analysis (above:IN12042).

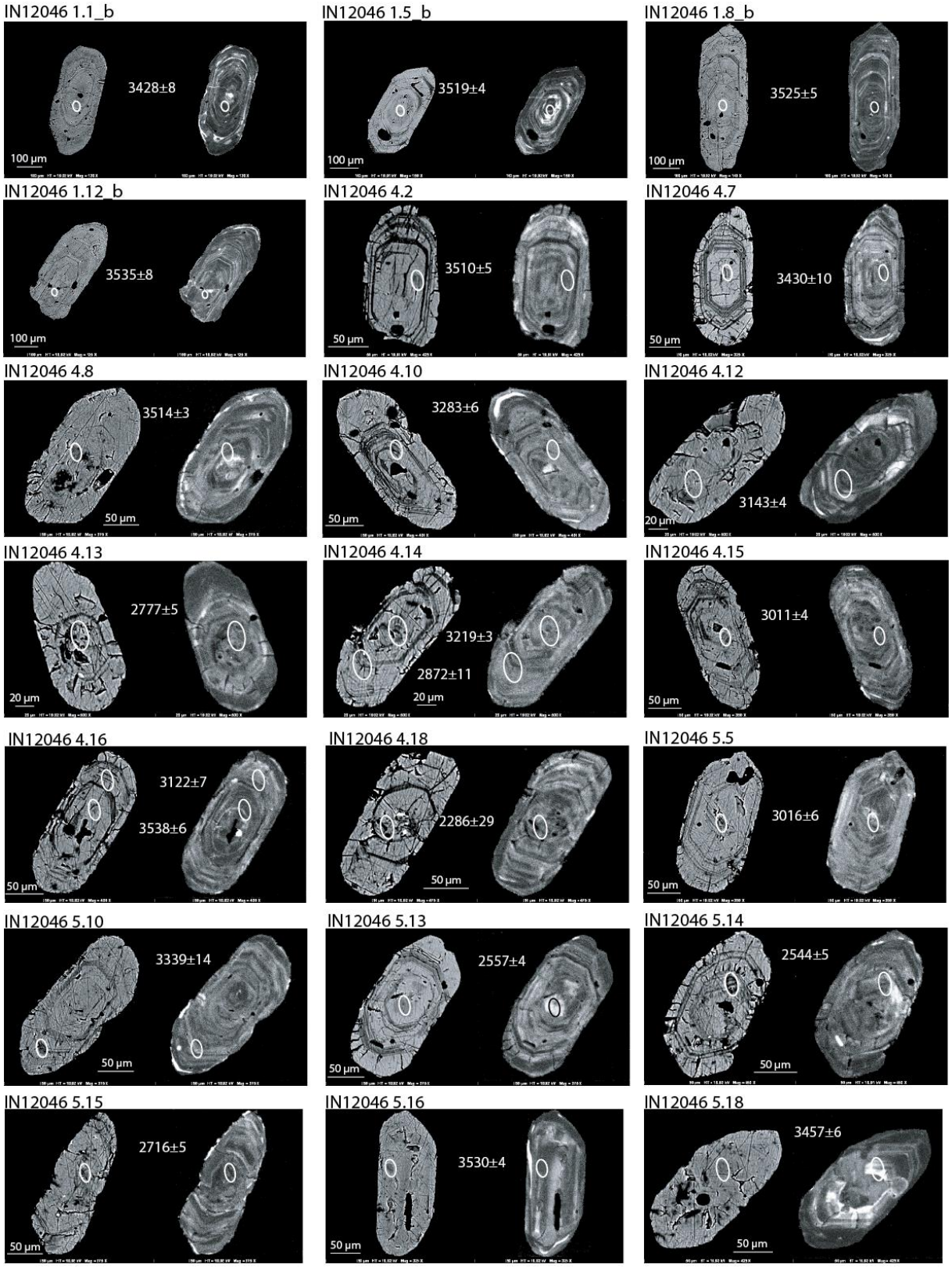

Figure 7. Backscatter electron and cathodoluminescence pared images of zircon grains used in geochronological and trace-element analysis (above: IN12046).

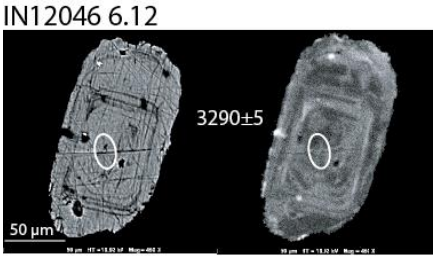

Figure 7. Backscatter electron and cathodoluminescence pared images of zircon grains used in geochronological and trace-element analysis (above: IN12046 cont.).

Figure 7. Backscatter electron and cathodoluminescence pared images of zircon grains used in geochronological and trace-element analysis (above: IN12050).

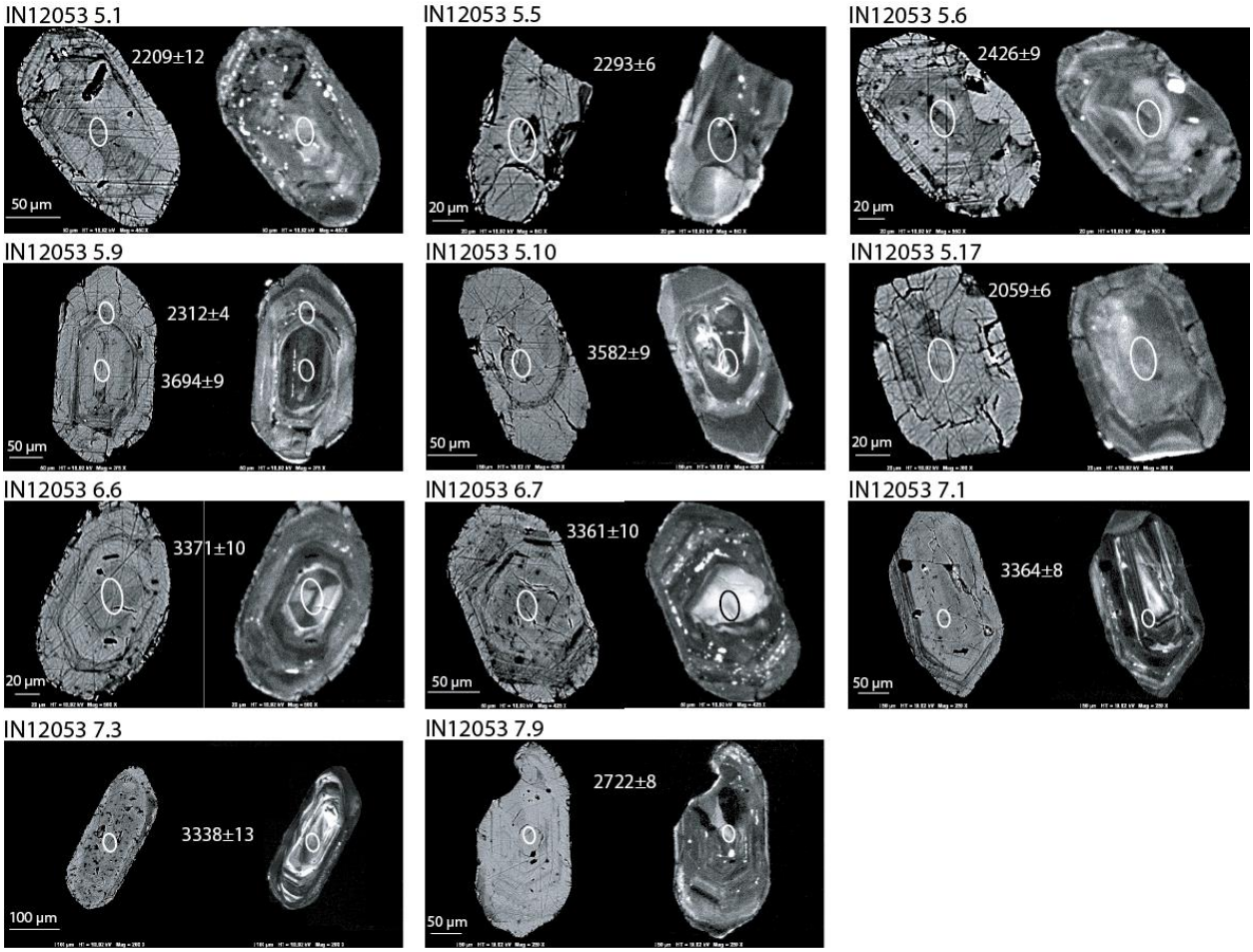

Figure 7. Backscatter electron and cathodoluminescence pared images of zircon grains used in geochronological and trace-element analysis (above: IN12053).

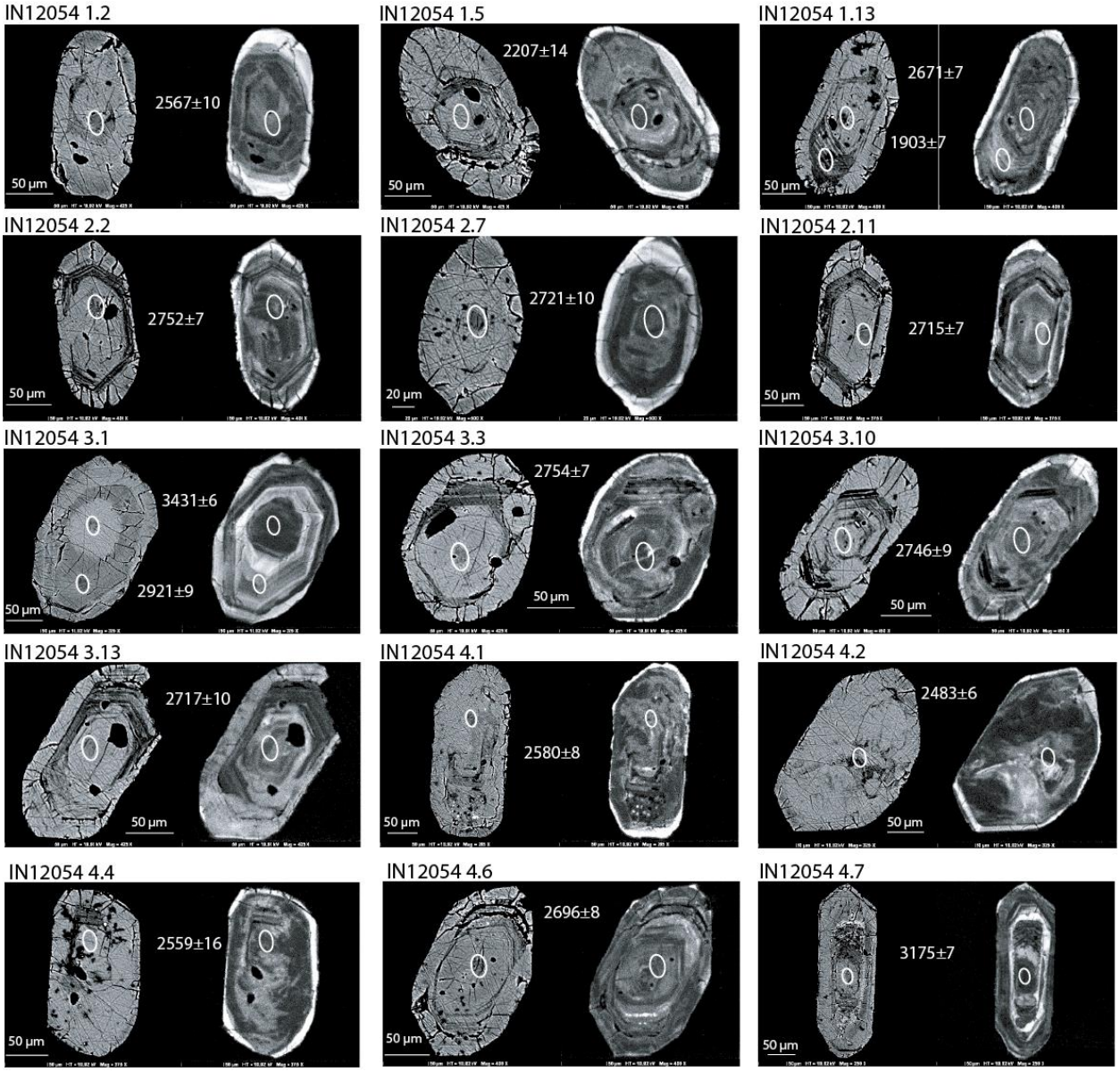

Figure 7. Backscatter electron and cathodoluminescence pared images of zircon grains used in geochronological and trace-element analysis (above: IN12054).

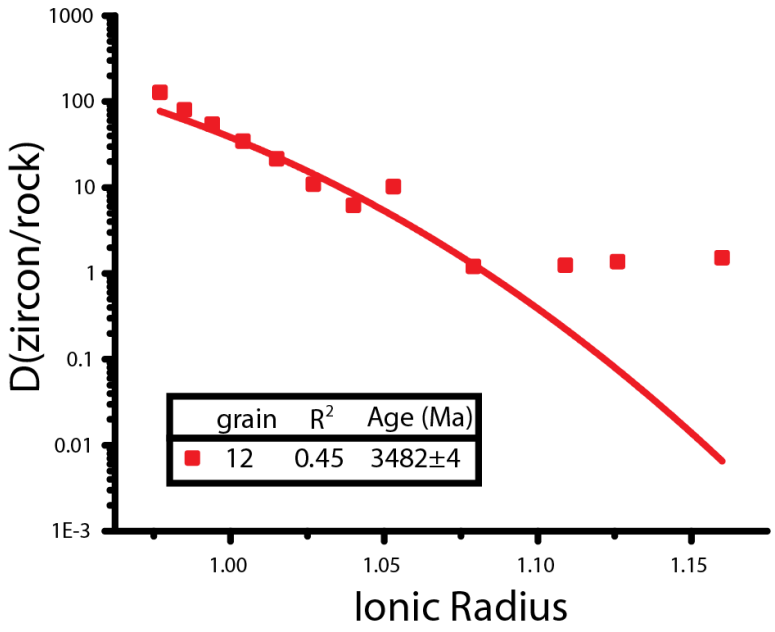

Figure 8a. Onuma diagram coupled with lattice strain partition modeling result of selected zircon from sample IN05001, using $Zircon_{REE}$/Host $rock_{REE}$ as the partitioning parameter.

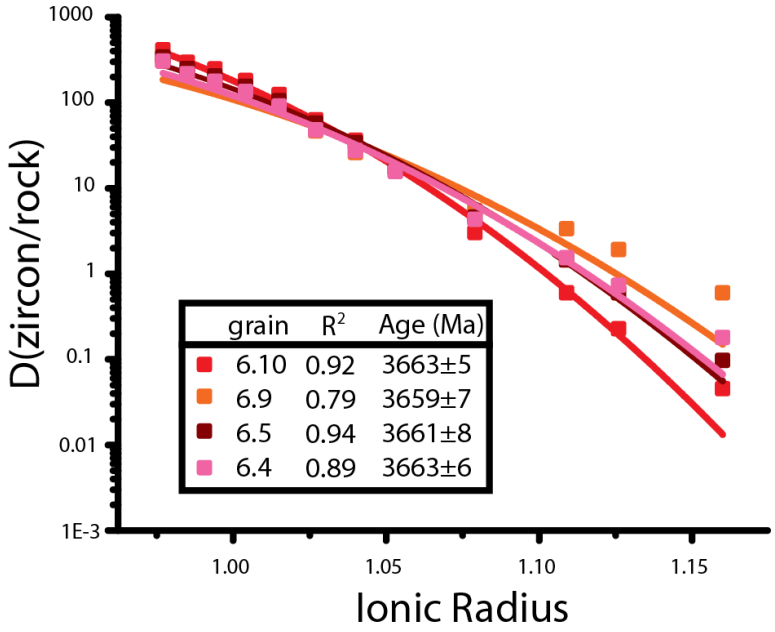

Figure 8b. Onuma diagram coupled with lattice strain partition modeling result of selected zircon from sample IN12012, using $Zircon_{REE}$/Host $rock_{REE}$ as the partitioning parameter.

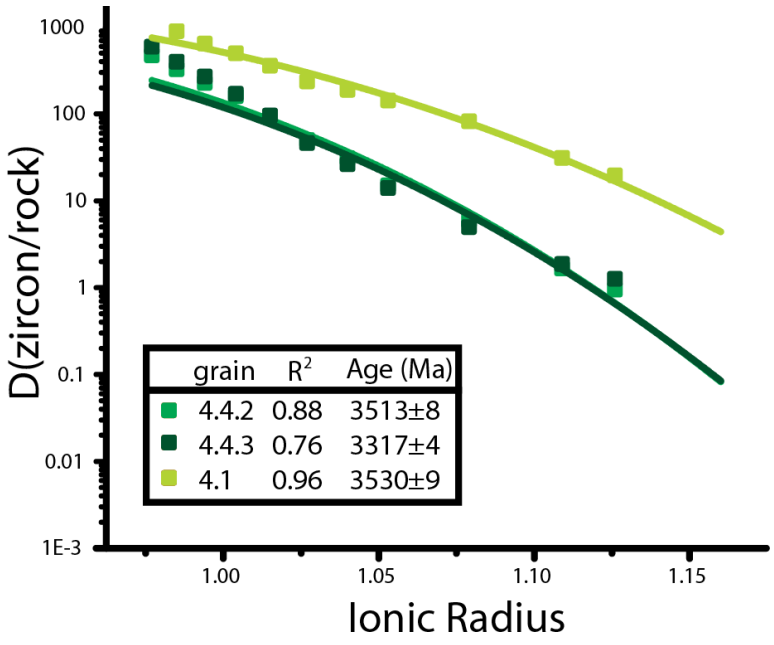

Figure 8c. Onuma diagram coupled with lattice strain partition modeling result of selected zircon from sample IN12027, using $Zircon_{REE}$/Host $rock_{REE}$ as the partitioning parameter.

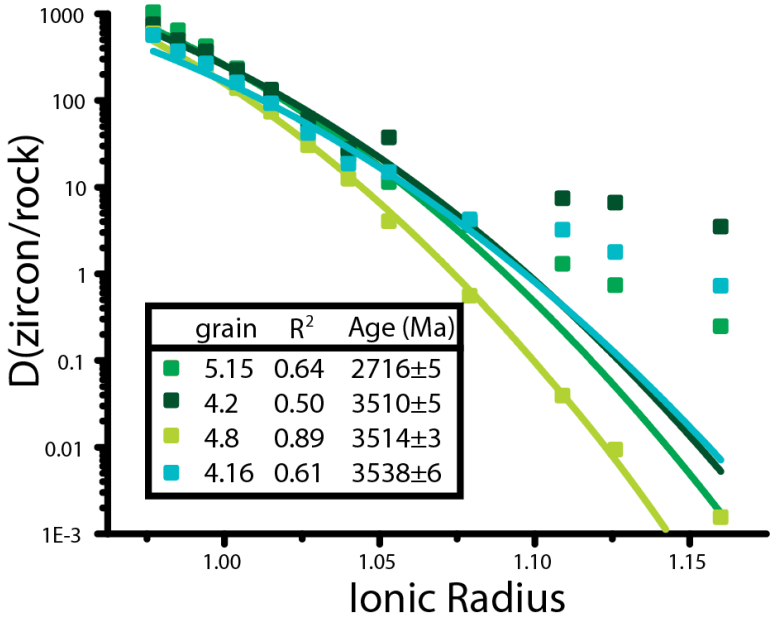

Figure 8d. Onuma diagram coupled with lattice strain partition modeling result of selected zircon from sample IN12046, using $Zircon_{REE}$/Host $rock_{REE}$ as the partitioning parameter.

Tables

Table 1. Data used for geochemical analysis; oxides reported in weight percentages and trace elements in ppm; CTG = red, Voizel = green, Boizard = blue, USB enclaves = purple

Sample	IN05001	IN12012	IN12014	IN12027	IN12041	IN12046	IN12050	IN12016	IN12054	IN12017	IN12042	IN12053
SiO_2	69.91	64.57	71.27	70.19	64.61	69.86	70.23	68.93	68.03	71.79	71.24	68.62
TiO_2	0.50	0.52	0.17	0.41	0.57	0.40	0.20	0.30	0.37	0.42	0.35	0.30
Al_2O_3	14.81	14.50	15.90	13.98	14.62	13.92	15.11	14.33	14.60	14.13	13.76	14.64
Fe_2O_3	4.22	5.84	1.94	3.86	6.10	3.87	1.62	3.82	3.67	2.61	3.46	3.60
MnO	0.07	0.11	0.02	0.07	0.10	0.05	0.02	0.08	0.04	0.02	0.05	0.05
MgO	1.13	3.42	0.59	1.47	2.98	1.50	0.69	1.56	1.11	1.68	1.06	0.95
CaO	3.38	4.52	3.11	2.26	3.60	3.58	2.04	2.58	1.76	3.15	2.25	2.36
Na_2O	3.54	3.12	4.39	3.15	3.58	3.34	3.01	3.67	3.33	4.00	3.16	3.74
K_2O	1.80	1.97	2.10	3.55	2.20	1.82	4.65	4.25	4.57	1.32	3.19	3.92
P_2O_5	0.14	0.17	< L.D.	0.09	0.08	0.12	0.06	0.04	0.16	0.09	0.09	0.08
PF		1.35	0.75	0.93	1.27	0.79	1.02	0.98	1.01	1.11	0.65	0.76
Total	100.15	100.08	100.22	99.95	99.69	99.25	98.63	100.51	98.65	100.32	99.25	99.01
Cr	8.28	78.4	9.9	24.5	82.7	28.0	4.7	92.4	19.2	55.8	19.3	11.9
Ni	5.2	50.9	8.8	19.5	53.7	21.9	6.6	73.5	13.0	50.9	12.2	17.0
Cu	15.5	40.65	25.13	27.67	34.53	31.39	25.54	13.32	17.52	48.29	< L.D.	8.236
Zn	50.5	65.5	27.8	79.6	91.7	54.4	22.2	60.2	56.7	30.3	75.4	51.2
Co		16.4	4.03	9.03	17.3	10.7	4.90	8.38	6.94	10.4	6.97	5.72
Ga	18.0	17.5	19.8	15.7	18.3	19.5	17.1	18.9	20.6	16.4	15.6	20.4
Rb	81.2	68.6	95.8	87.3	99.5	109.7	121.1	134.5	139.2	66.7	94.5	104.5
Sr		284.0	230.8	157.8	146.7	174.9	315.6	290.6	440.4	207.0	121.7	336.9
Y	19.4	16.5	3.18	7.90	14.3	13.4	2.15	14.8	7.06	8.00	5.93	10.7
Zr	298	137.4	148.4	164.7	148.4	257.1	183.9	39.3	270.0	197.6	173.3	111.3
Nb	13.1	6.36	9.26	6.68	6.83	10.3	2.84	7.84	3.64	8.24	5.62	6.44
Mo	0.53	3.282	< L.D.	< L.D.	< L.D.	< L.D.	< L.D.	< L.D.	< L.D.	0.547	< L.D.	< L.D.
Sn	2.30	1.865	< L.D.	1.015	1.227	1.035	0.505	1.475	0.996	< L.D.	0.829	1.022
Sb	0.02	< L.D.	< L.D.	< L.D.	< L.D.	< L.D.	< L.D.	< L.D.	< L.D.	< L.D.	< L.D.	< L.D.
Cs	2.98	1.471	0.592	2.452	2.254	0.945	0.703	0.305	0.42	1.09	1.518	0.145
Ba		427.5	272.3	694.6	262.5	264.9	1903.0	965.3	1844.0	133.9	564.9	875.1
La	56.1	32.1	49.3	10.9	30.5	52.7	27.0	15.1	127.2	22.9	34.7	14.8
Ce	91.6	60.2	92.1	19.8	51.5	92.7	43.9	30.7	227.9	37.6	55.1	33.4
Pr	8.91	6.70	8.54	2.06	5.10	9.00	4.01	3.70	20.1	3.68	5.00	3.73
Nd	30.1	24.9	26.5	7.46	17.8	28.4	12.6	14.7	59.5	12.5	15.4	14.4
Sm	4.74	4.55	3.35	1.51	3.31	4.08	1.72	3.39	6.30	2.16	2.12	2.95
Eu	0.96	1.29	0.71	0.95	0.82	0.80	0.96	0.74	0.89	0.72	0.95	0.79
Gd	3.83	3.48	2.01	1.44	2.94	3.24	1.13	2.83	4.07	1.83	1.77	2.28
Tb	0.57	0.49	0.19	0.22	0.44	0.44	0.12	0.44	0.40	0.26	0.22	0.32
Dy	3.45	2.87	0.79	1.33	2.59	2.35	0.50	2.62	1.72	1.41	1.14	1.82
Ho	0.69	0.54	0.11	0.26	0.50	0.45	0.08	0.50	0.25	0.27	0.21	0.35
Er	2.11	1.55	0.30	0.74	1.37	1.27	0.21	1.37	0.66	0.73	0.56	0.98
Tm	0.31	0.23	0.04	0.12	0.20	0.18	0.03	0.20	0.08	0.11	0.08	0.15
Yb	2.11	1.58	0.31	0.75	1.35	1.22	0.23	1.24	0.51	0.71	0.49	0.96
Lu	0.337	0.25	0.06	0.13	0.21	0.19	0.04	0.18	0.08	0.12	0.08	0.15

Hf	6.91	3.41	4.22	3.93	3.75	6.32	4.55	1.25	6.75	4.87	4.33	3.31
Ta	4.58	0.52	0.56	0.27	0.47	0.88	0.13	0.58	0.12	0.70	0.27	0.24
Pb	13.7	13.3	26.6	12.1	14.1	14.6	19.7	16.5	21.5	12.5	22.1	21.4
Bi	0.045	0.128	< L.D.	< L.D.	< L.D.	< L.D.	< L.D.	< L.D.	< L.D.	< L.D.	0.108	< L.D.
Th	16.25	8.18	40.5	1.77	8.85	19.9	10.4	4.53	34.0	8.52	5.01	8.90
U	4.21	1.17	1.64	0.50	0.67	1.01	0.45	0.28	0.73	1.33	0.51	0.76
As		< L.D.	< L.D.	< L.D.	< L.D.	< L.D.	< L.D.	< L.D.	< L.D.	< L.D.	< L.D.	< L.D.
Be	2.21	1.478	2.178	1.202	1.524	2.092	1.432	1.602	1.22	1.945	1.269	1.491
Cd		0.212	0.14	0.204	0.302	0.248	0.159	< L.D.	0.197	0.214	0.191	0.163
Ge		1.42	0.90	1.00	1.21	1.44	1.00	1.22	1.43	0.99	1.15	1.28
In		< L.D.	< L.D.	< L.D.	< L.D.	< L.D.	< L.D.	< L.D.	< L.D.	< L.D.	< L.D.	< L.D.
V	39	89.4	13.3	48.2	103.6	50.3	16.7	37.3	42.6	37.2	31.1	26.8
W		0.349	< L.D.	< L.D.	< L.D.	< L.D.	< L.D.	< L.D.	< L.D.	< L.D.	0.471	< L.D.
Th/U	3.86	6.98	24.66	3.53	13.17	19.67	23.04	16.45	46.65	6.40	9.84	11.77
$[Th/U]_{Zr}$[1]	0.77	1.40	4.93	0.71	2.63	3.93	4.61	3.29	9.33	1.28	1.97	2.35
Y/Ho	28.16	30.28	28.17	30.03	28.57	30.07	28.33	29.80	28.12	29.42	28.35	30.34
M[2]	1.42	1.74	1.43	1.41	1.65	1.50	1.35	1.66	1.43	1.44	1.36	1.54
$T_{zr}(^oC)$[3]	825.15	731.65	762.86	773.31	744.98	804.14	787.98	647.90	815.01	786.48	781.65	730.98
Total REE	205.81	140.65	184.31	47.63	118.56	196.98	92.47	77.66	449.66	85.05	117.75	77.13

[1] Predicted Th/U ratio zircon crystallizing from a melt with the Th/U ratio of the rock. Assumes 0.2 partition coefficient.
[2] Calculated M value for zircon saturation, using the formula of Watson and Harrison (1983).
[3] Zircon saturation temperature for each lithology, using the the formula of Watson and Harrison (1983).

Chondrite Normalization (Anders and Grevesse, 1989)

Sample	IN05001	IN12012	IN12014	IN12027	IN12041	IN12046	IN12050	IN12016	IN12054	IN12017	IN12042	IN12053
La	239.029	136.557	209.842	46.570	129.953	224.414	114.870	64.337	541.968	97.742	147.806	63.102
Ce	151.857	99.834	152.735	32.742	85.295	153.614	72.712	50.845	377.818	62.334	91.263	55.421
Pr	100.000	75.208	95.836	23.098	57.273	101.021	44.983	41.526	225.926	41.257	56.061	41.852
Nd	66.511	54.929	58.621	16.483	39.257	62.865	27.918	32.449	131.432	27.697	34.063	31.874
Pm												
Sm	32.202	30.925	22.774	10.252	22.529	27.716	11.713	23.059	42.808	14.670	14.398	20.034
Eu	17.143	23.107	12.732	16.893	14.679	14.339	17.071	13.286	15.893	12.857	16.929	14.089
Gd	19.481	17.675	10.214	7.304	14.964	16.495	5.768	14.405	20.697	9.303	8.983	11.617
Tb	15.702	13.554	5.207	5.950	11.983	11.983	3.306	12.066	11.102	7.135	5.923	8.926
Dy	14.215	11.817	3.259	5.496	10.680	9.691	2.064	10.799	7.083	5.797	4.701	7.478
Ho	12.410	9.784	2.032	4.730	9.029	8.004	1.367	8.957	4.514	4.892	3.759	6.313
Er	13.285	9.755	1.888	4.657	8.634	7.961	1.303	8.597	4.179	4.600	3.518	6.167
Tm	12.874	9.587	1.653	4.835	8.430	7.479	1.281	8.099	3.264	4.339	3.182	6.074
Yb	13.004	9.711	1.902	4.609	8.314	7.495	1.385	7.643	3.163	4.345	2.997	5.908
Lu	13.858	10.329	2.346	5.144	8.807	7.737	1.687	7.449	3.292	4.897	3.457	5.967
La/Yb	18.381	14.062	110.354	10.104	15.631	29.940	82.962	8.418	171.342	22.497	49.319	10.681
Gd/Yb	1.498	1.820	5.371	1.585	1.800	2.201	4.166	1.885	6.543	2.141	2.997	1.967
La/Sm	7.423	4.416	9.214	4.543	5.768	8.097	9.807	2.790	12.661	6.663	10.265	3.150
Eu/Eu*	0.663	0.951	0.772	1.924	0.783	0.649	1.953	0.709	0.501	1.073	1.448	0.890
Ce_N/Yb_N	11.678	10.281	80.322	7.104	10.259	20.494	52.514	6.652	119.446	14.347	30.452	9.381
K	1.492	1.636	1.740	2.944	1.830	1.514	3.856	3.524	3.794	1.097	2.651	3.253

Primative Mantle Normalization (McDonough, 1992)

Sample	IN05001	IN12012	IN12014	IN12027	IN12041	IN12046	IN12050	IN12016	IN12054	IN12017	IN12042	IN12053
Rb	127.90	108.08	150.80	137.43	156.72	172.76	190.71	211.81	219.21	105.06	148.87	164.57
Ba	0.00	61.16	38.96	99.37	37.55	37.90	272.25	138.10	263.81	19.16	80.82	125.19
K	62.16	68.18	72.50	122.65	76.24	63.09	160.67	146.83	158.07	45.73	110.48	135.56
Th	193.51	97.35	482.62	21.07	105.32	236.31	123.45	53.87	404.88	101.42	59.61	105.96
Nb	18.38	8.92	12.98	9.37	9.58	14.40	3.99	10.99	5.11	11.56	7.89	9.04
La	79.24	45.27	69.56	15.44	43.08	74.39	38.08	21.33	179.66	32.40	49.00	20.92
Ce	49.97	32.85	50.26	10.77	28.07	50.55	23.93	16.73	124.33	20.51	30.03	18.24
Sr	0.00	13.46	10.94	7.48	6.95	8.29	14.96	13.77	20.87	9.81	5.77	15.97
Nd	22.03	18.19	19.41	5.46	13.00	20.82	9.25	10.75	43.53	9.17	11.28	10.56
Zr	26.59	12.27	13.25	14.71	13.25	22.96	16.42	3.51	24.11	17.64	15.47	9.94
Eu	5.71	7.70	4.24	5.63	4.89	4.78	5.69	4.43	5.30	4.29	5.64	4.70
Ti	2.36	2.45	0.78	1.92	2.66	1.89	0.93	1.39	1.74	1.98	1.62	1.39
Dy	4.68	3.89	1.07	1.81	3.52	3.19	0.68	3.56	2.33	1.91	1.55	2.46
Y	4.27	3.62	0.70	1.74	3.15	2.94	0.47	3.26	1.55	1.76	1.30	2.34
Er	4.41	3.24	0.63	1.54	2.86	2.64	0.43	2.85	1.39	1.53	1.17	2.05
Yb	4.40	3.29	0.64	1.56	2.81	2.54	0.47	2.59	1.07	1.47	1.01	2.00
Zr/Zr*	1.92	0.95	1.12	2.65	1.48	1.79	2.20	0.46	0.99	2.62	1.83	1.30
Nb/Nb*	0.13	0.13	0.05	0.51	0.13	0.09	0.05	0.29	0.02	0.17	0.15	0.14
Ti/Ti*	0.58	0.48	0.31	0.51	0.70	0.57	0.28	0.48	0.49	0.63	0.45	0.46

Total Alkali Concentration

Sample	IN05001	IN12012	IN12014	IN12027	IN12041	IN12046	IN12050	IN12016	IN12054	IN12017	IN12042	IN12053
K_2O	1.80	1.97	2.10	3.55	2.20	1.82	4.65	4.25	4.57	1.32	3.19	3.92
Al_2O_3	14.81	14.50	15.90	13.98	14.62	13.92	15.11	14.33	14.60	14.13	13.76	14.64
$CaO+Na_2O$	6.92	7.63	7.50	5.41	7.18	6.92	5.05	6.25	5.09	7.15	5.42	6.10
Total	8.72	9.61	9.59	8.96	9.38	8.74	9.70	10.50	9.66	8.47	8.61	10.02

Table 2. Data used for geochronological analysis, organized by sample number

Name	Age (Ma) $^{207}Pb/^{206}Pb$	Age (Ma) $^{207}Pb/^{206}Pb$ 1 s.e.	% Concordant	$^{238}U/^{206}Pb$	$^{238}U/^{206}Pb$ 1 s.e.	$^{207}Pb^*/^{206}Pb^*$	$^{207}Pb^*/^{206}Pb^*$ 1 s.e.	Th/U	Th/U 1 s.e.
IN05001 4_12	3482	4.29	98.3	1.421	0.061	3.02E-01	8.38E-04	0.1983	2.39E-03
IN05001 4_13	3320	5.81	85.0	1.747	0.060	2.72E-01	1.01E-03	0.3604	6.16E-03
IN05001 4_14	2648	22.5	74.3	2.649	0.112	1.80E-01	2.43E-03	0.2512	3.50E-03
IN05001 4_15	3282	7.14	87.0	1.732	0.073	2.66E-01	1.21E-03	0.1562	2.94E-03
IN05001 4_16	3338	17.8	81.3	1.813	0.076	2.76E-01	3.14E-03	0.271	1.99E-03
IN05001 4_17	3424	6.18	69.5	2.053	0.076	2.91E-01	1.16E-03	0.4824	4.79E-03
IN05001 4_18	3492	4.55	97.6	1.425	0.064	3.04E-01	8.95E-04	0.3291	2.15E-03
IN05001 4_19	3486	3.95	98.1	1.421	0.063	3.03E-01	7.74E-04	9.38E-02	1.49E-03
IN05001 4_1	3338	9.33	98.3	1.500	0.062	2.76E-01	1.64E-03	0.4086	3.87E-03
IN05001 4_2	3457	5.51	87.6	1.609	0.070	2.98E-01	1.06E-03	0.3161	3.19E-03
IN05001 4_3	3591	4.7	99.2	1.353	0.058	3.24E-01	9.92E-04	0.6342	4.36E-03
IN05001 4_5	3474	6.02	96.2	1.456	0.065	3.01E-01	1.17E-03	0.5288	2.18E-03
IN05001 4_6	2994	20.5	73.2	2.309	0.090	2.22E-01	2.83E-03	0.2843	2.23E-03
IN05001 4_7	3041	5.75	83.1	1.996	0.084	2.28E-01	8.20E-04	0.5074	6.58E-03
IN05001 4_8	2985	9.12	74.1	2.293	0.121	2.21E-01	1.25E-03	6.34E-02	1.50E-03
IN05001 4_9	3475	4.7	96.5	1.450	0.062	3.01E-01	9.14E-04	0.3242	5.08E-03
IN05001 4_10	3446	8.11	93.0	1.522	0.066	2.95E-01	1.54E-03	0.2063	1.82E-03
IN05001 5_1	2884	9.5	91.3	1.942	0.070	2.07E-01	1.21E-03	0.1277	3.47E-03
IN05001 5_2	3512	5.48	92.9	1.487	0.053	3.08E-01	1.09E-03	0.5725	4.23E-03
IN05001 5_3	2862	13.9	75.8	2.360	0.100	2.05E-01	1.75E-03	0.2651	1.69E-03
IN05001 5_4	3490	12.6	97.0	1.435	0.061	3.04E-01	2.47E-03	0.2291	4.80E-03
IN05001 5_5	3364	4.15	87.1	1.676	0.060	2.80E-01	7.45E-04	0.2484	2.41E-03
IN05001 5_6	2734	6.91	95.6	1.980	0.078	1.89E-01	7.93E-04	0.1474	3.38E-03
IN05001 5_7	3459	6.06	93.4	1.508	0.062	2.98E-01	1.17E-03	0.1934	7.24E-03
IN05001 5_8	3533	5.7	95.5	1.434	0.053	3.12E-01	1.15E-03	0.559	5.16E-02
IN05001 5_10	3300	170	101.3	1.477	0.057	2.69E-01	2.92E-02	0.2469	3.89E-03
IN12012 6_4	3663	6.38	103.3	1.266	0.064	0.340	0.00142	1.627	1.66E-02
IN12012 6_5	3661	7.92	100.9	1.297	0.067	0.340	0.00176	1.687	2.16E-02
IN12012 6_8	3466	7.11	102.8	1.366	0.073	0.299	0.00137	0.082	1.54E-03
IN12012 6_9	3659	6.91	103.6	1.263	0.066	0.339	0.00153	1.644	1.76E-02
IN12012 6_10	3663	5.09	100.1	1.306	0.059	0.340	0.00113	1.559	8.49E-03
IN12012 6_11	3583	9.36	97.0	1.387	0.079	0.323	0.00197	1.366	1.59E-02
IN12012 6_14	3658	4.45	105.2	1.244	0.059	0.339	0.00099	1.799	1.47E-02
IN12012 6_15	3615	16	102.0	1.304	0.069	0.330	0.00344	0.496	1.14E-02
IN12012 6_16	3619	9.37	95.1	1.396	0.068	0.331	0.00202	1.011	1.98E-02
IN12012 6_19	3636	10	99.3	1.329	0.063	0.334	0.00219	1.706	1.72E-02
IN12012 7_9	3507	3.74	99.6	1.389	0.060	0.307	0.00075	1.624	1.18E-02

IN12012 7_8	3325	8.92	89.7	1.652	0.065	0.273	0.00156	1.722	1.29E-02
IN12012 7_4	3102	6.1	86.3	1.874	0.083	0.237	0.00091	0.275	4.99E-03
IN12012 7_2	3662	8.28	109.7	1.192	0.057	0.340	0.00184	1.547	1.34E-02
IN12012 7_1	3655	11.4	107.2	1.223	0.077	0.338	0.00251	1.440	2.25E-02
IN12014 b_6_1	3458	6.19	88.9	1.585	0.066	0.298	0.00119	0.131	2.09E-03
IN12014 b_6_2	3275	13.9	76.8	1.967	0.082	0.265	0.00233	0.278	5.34E-03
IN12014 b_6_3	2924	54.8	56.5	3.082	0.153	0.212	0.00719	1.538	2.33E-02
IN12014 b_6_4	2933	7.08	68.6	2.530	0.099	0.214	0.00094	0.108	2.09E-03
IN12014 b_6_6	1925	12.3	74.5	3.855	0.156	0.118	0.00081	0.225	2.32E-03
IN12014 b_6_11	3341	3.87	80.5	1.829	0.065	0.276	0.00068	0.062	1.09E-03
IN12014 b_6_9	3482	33.1	82.4	1.695	0.144	0.302	0.00647	9.567	3.03E-01
IN12014 b_6_8	1925	10.3	58.7	4.895	0.189	0.118	0.00068	0.227	1.79E-03
IN12014 b_6_6_2	1818	9.23	74.6	4.117	0.171	0.111	0.00057	0.240	2.28E-03
IN12014 b_6_4_2	1849	9.62	67.3	4.476	0.169	0.113	0.00060	0.253	2.59E-03
IN12014 4_12	2867	8.02	68.7	2.600	0.128	0.205	0.00101	0.056	8.51E-04
IN12014 4_18	3504	9.97	95.4	1.451	0.071	0.307	0.00198	0.774	2.92E-03
IN12014 4_19	2661	6.77	63.6	3.075	0.141	0.181	0.00074	0.343	5.03E-03
IN12014 4_20	2735	14	71.4	2.651	0.122	0.189	0.00161	0.297	1.88E-02
IN12016 b_5_12	2427	6.31	60.5	3.617	0.127	0.157	0.00059	0.142	3.18E-03
IN12016 b_5_11	2572	18.6	66.1	3.087	0.122	0.171	0.00190	0.065	1.18E-03
IN12016 b_5_11_2	2692	11.3	89.4	2.159	0.094	0.184	0.00126	0.852	7.48E-03
IN12016 b_5_9	3063	17	53.9	3.051	0.101	0.232	0.00246	0.084	1.39E-03
IN12016 b_5_6	2553	9.53	63.6	3.237	0.118	0.170	0.00097	0.134	3.54E-03
IN12016 b_5_5	2778	8.5	53.4	3.479	0.125	0.194	0.00101	0.066	1.37E-03
IN12016 b_5_5_2	2704	11.2	96.2	1.995	0.085	0.186	0.00127	0.802	1.21E-02
IN12016 b_5_4	2005	9.08	62.9	4.357	0.165	0.123	0.00063	0.161	4.15E-03
IN12016 b_5_3	2569	6.6	82.1	2.489	0.107	0.171	0.00068	0.037	9.36E-04
IN12016 b_5_3_2	1988	10.9	50.6	5.470	0.219	0.122	0.00075	0.208	2.15E-03
IN12016 b_5_2	2685	7.8	93.4	2.072	0.086	0.184	0.00087	0.459	8.65E-03
IN12016 b_5_1	2027	8.68	66.6	4.067	0.170	0.125	0.00061	0.128	8.43E-04
IN12016 6_2	3047	8.48	87.4	1.893	0.074	0.229	0.00121	0.755	9.24E-03
IN12016 6_3	3007	6.55	95.8	1.756	0.064	0.224	0.00091	0.032	9.63E-04
IN12016 6_6	2434	4.36	84.4	2.584	0.091	0.158	0.00041	0.162	3.84E-03
IN12016 6_9	3332	12.1	92.7	1.594	0.078	0.275	0.00212	0.819	1.25E-02
IN12016 6_9_2	2443	9.18	76.1	2.853	0.123	0.159	0.00086	0.177	4.10E-03
IN12016 6_10	3212	6.84	72.3	2.141	0.074	0.254	0.00110	0.033	1.18E-03
IN12016 6_11	2731	6.73	90.0	2.106	0.071	0.189	0.00077	0.616	6.26E-03
IN12016 6_11_2	3365	12.1	96.4	1.514	0.101	0.280	0.00217	0.713	2.16E-02
IN12016 6_12	1751	8.38	67.4	4.755	0.168	0.107	0.00049	0.377	2.43E-03
IN12016 6_14	3078	25.2	79.2	2.062	0.091	0.234	0.00368	0.161	7.15E-03
IN12016 6_18	2705	8.22	100.5	1.908	0.080	0.186	0.00093	0.837	1.23E-02

IN12016 6_19	2465	14.1	53.2	4.039	0.144	0.161	0.00135	0.093	1.58E-03
IN12016 5_22	3704	12.6	98.2	1.311	0.052	0.349	0.00290	0.067	8.34E-03
IN12016 5_4	2700	8.28	100.1	1.920	0.077	0.185	0.00093	0.039	1.09E-03
IN12016 5_1	3032	7.11	87.5	1.903	0.073	0.227	0.00101	0.029	9.99E-04
IN12017 1_1	2132	11.8	59.3	4.301	0.182	0.133	0.00089	0.127	4.76E-03
IN12017 1_2	2082	9.62	68.7	3.817	0.168	0.129	0.00070	0.075	9.59E-04
IN12017 1_4	3495	6.14	91.7	1.515	0.068	0.305	0.00121	0.165	2.06E-03
IN12017 1_6	2828	4.55	59.2	3.067	0.124	0.200	0.00056	0.028	4.15E-04
IN12017 1_7	2923	7.23	62.3	2.798	0.106	0.212	0.00095	0.226	8.64E-03
IN12017 1_8	2571	25.7	62.6	3.259	0.134	0.171	0.00264	0.080	1.89E-03
IN12017 1_14	3071	4.8	88.5	1.852	0.074	0.233	0.00070	0.092	1.75E-03
IN12017 1_18	3653	8	105.2	1.247	0.065	0.338	0.00177	0.738	7.45E-03
IN12027 b_4_1	3530	8.67	99.3	1.382	0.062	0.312	0.00175	0.689	5.24E-03
IN12027 b_4_1_2	3299	8.55	84.2	1.778	0.081	0.269	0.00147	0.372	4.29E-03
IN12027 b_4_2	3289	10.9	76.0	1.977	0.072	0.267	0.00186	0.398	3.23E-03
IN12027 b_4_3	3482	8.93	84.9	1.645	0.058	0.302	0.00174	0.301	3.94E-03
IN12027 b_4_4	3509	6.09	93.3	1.482	0.056	0.308	0.00121	0.379	6.39E-03
IN12027 b_4_4_2	3513	7.93	96.8	1.426	0.062	0.308	0.00158	0.395	4.00E-03
IN12027 b_4_4_3	3317	4.35	78.1	1.902	0.098	0.272	0.00075	0.338	4.23E-03
IN12027 2_1	3425	6.55	83.4	1.709	0.089	0.291	0.00123	0.753	9.29E-03
IN12027 2_2	2962	4.39	82.1	2.089	0.109	0.217	0.00059	0.338	2.57E-03
IN12027 2_4	3225	5.08	79.0	1.951	0.089	0.256	0.00083	0.361	2.45E-03
IN12027 2_5	3181	11.2	79.4	1.973	0.115	0.249	0.00176	0.531	2.18E-02
IN12027 2_7	3061	4.54	86.2	1.909	0.101	0.231	0.00066	0.413	2.61E-03
IN12027 2_10	3052	4.41	83.7	1.972	0.103	0.230	0.00063	0.383	3.68E-03
IN12027 2_11	3527	6.53	87.7	1.566	0.070	0.311	0.00132	0.385	6.21E-03
IN12027 2_13	3106	15.8	84.5	1.912	0.111	0.238	0.00236	0.207	7.77E-03
IN12041 b_3_1	2175	30.4	75.6	3.296	0.125	0.136	0.00237	0.540	3.87E-03
IN12041 b_3_1_2	3354	13.1	69.1	2.120	0.085	0.278	0.00233	0.628	1.00E-02
IN12041 b_3_2	3338	105	84.2	1.750	0.085	0.276	0.01860	0.527	6.84E-03
IN12041 b_3_4	3341	16.2	82.3	1.790	0.076	0.276	0.00287	0.496	3.70E-03
IN12041 b_3_4_2	3356	4.63	85.7	1.708	0.058	0.279	0.00083	0.351	3.37E-03
IN12041 b_3_5	3516	7.74	94.1	1.466	0.059	0.309	0.00155	0.521	9.03E-03
IN12041 3_19	3161	6.07	92.4	1.710	0.073	0.246	0.00094	0.677	1.13E-02
IN12041 3_15	3244	11.2	86.8	1.762	0.084	0.260	0.00185	0.440	2.80E-03
IN12041 3_9	3172	16.6	77.2	2.039	0.088	0.248	0.00260	0.476	5.56E-03
IN12041 3_5	3507	4.31	92.3	1.499	0.058	0.307	0.00086	0.820	5.91E-03
IN12041 3_1	3448	4.84	91.0	1.553	0.055	0.296	0.00092	1.063	4.55E-03
IN12041 4_2	2580	8.93	80.0	2.539	0.101	0.172	0.00092	0.208	3.30E-03
IN12041 4_5	3306	7.71	76.6	1.948	0.068	0.270	0.00133	0.308	3.20E-03

IN12041 4_8	3388	5.7	85.0	1.702	0.066	0.285	0.00104	0.447	4.79E-03
IN12042 b_2_1	3423	6.75	105.4	1.354	0.059	0.291	0.00126	0.757	1.13E-02
IN12042 b_2_3	3144	14	67.7	2.349	0.094	0.244	0.00215	0.425	6.51E-03
IN12042 b_2_4	3454	8.92	94.9	1.486	0.057	0.297	0.00171	0.342	5.85E-03
IN12042 b_2_4_2	3333	4.86	79.0	1.870	0.067	0.275	0.00085	0.302	3.38E-03
IN12042 b_2_10	3529	8.22	95.5	1.436	0.054	0.312	0.00166	0.672	6.40E-03
IN12042 b_2_12	2998	10	79.8	2.117	0.075	0.222	0.00139	0.334	3.31E-03
IN12046 b_1_12	3535	8.18	98.2	1.395	0.065	0.313	0.00166	0.616	8.66E-03
IN12046 b_1_8	3525	5.04	100.0	1.373	0.054	0.311	0.00102	0.414	4.81E-03
IN12046 b_1_5	3519	4.35	101.8	1.353	0.052	0.310	0.00087	0.368	5.68E-03
IN12046 b_1_1	3428	7.85	97.4	1.463	0.059	0.292	0.00148	0.718	9.22E-03
IN12046 6_12	3290	5.39	105.5	1.423	0.094	0.267	0.00092	0.262	2.94E-03
IN12046 5_18	3457	6.28	113.5	1.242	0.093	0.297	0.00120	0.369	4.34E-03
IN12046 5_16	3530	4.18	117.4	1.168	0.081	0.312	0.00085	0.636	5.75E-03
IN12046 5_15	2716	5.13	95.0	2.009	0.155	0.187	0.00058	0.704	5.37E-03
IN12046 5_14	2544	5.4	83.4	2.478	0.166	0.169	0.00054	0.213	1.02E-03
IN12046 5_13	2557	4.4	69.3	2.963	0.166	0.170	0.00045	0.222	1.19E-03
IN12046 5_10	3339	13.8	48.3	3.050	0.141	0.276	0.00243	0.500	6.76E-03
IN12046 5_5	3016	5.64	82.3	2.036	0.098	0.225	0.00079	0.680	1.15E-02
IN12046 4_2	3510	5.03	97.8	1.413	0.073	0.308	0.00100	0.460	1.02E-02
IN12046 4_7	3430	10.2	85.7	1.661	0.086	0.292	0.00191	0.446	1.30E-02
IN12046 4_8	3514	3.38	98.7	1.398	0.070	0.309	0.00068	0.338	2.56E-03
IN12046 4_10	3283	5.98	70.6	2.133	0.089	0.266	0.00101	0.412	4.15E-03
IN12046 4_12	3143	3.92	83.3	1.910	0.088	0.244	0.00060	0.664	2.65E-03
IN12046 4_13	2777	5.33	69.3	2.678	0.129	0.194	0.00063	0.751	4.83E-03
IN12046 4_14	3219	3.35	83.6	1.847	0.088	0.255	0.00054	0.385	3.50E-03
IN12046 4_14_2	2872	11.1	70.0	2.544	0.124	0.206	0.00140	0.686	6.10E-03
IN12046 4_15	3011	4.21	91.5	1.836	0.092	0.224	0.00059	0.389	3.16E-03
IN12046 4_16	3538	6.26	98.3	1.391	0.069	0.314	0.00127	0.514	5.68E-03
IN12046 4_16_2	3122	7.49	71.4	2.248	0.105	0.240	0.00113	0.414	2.38E-03
IN12046 4_20	3603	16	66.2	2.017	0.082	0.327	0.00341	0.824	2.29E-02
IN12046 4_18	2286	29.1	24.2	9.728	0.354	0.145	0.00245	6.246	6.94E-02
IN12050 5_18	2653	11.2	59.0	3.328	0.155	0.180	0.00122	0.101	5.52E-03
IN12050 5_15	3476	4.18	82.9	1.687	0.071	0.301	0.00081	0.071	1.46E-03
IN12050 5_14	3412	6.43	96.3	1.488	0.066	0.289	0.00119	0.530	6.20E-03
IN12050 5_13	2854	8.11	65.9	2.726	0.131	0.204	0.00101	0.077	1.02E-03
IN12050 5_11	3379	6.54	99.9	1.453	0.072	0.283	0.00119	0.207	2.98E-03
IN12050 5_9	2996	5.37	85.0	1.989	0.089	0.222	0.00074	0.354	3.22E-03
IN12050 5_8	2964	6.25	79.7	2.148	0.100	0.218	0.00084	0.168	1.55E-03
IN12050 5_7	3475	9.66	104.7	1.337	0.064	0.301	0.00188	0.486	7.13E-03

IN12050 5_5	2512	10.2	65.8	3.189	0.150	0.165	0.00101	0.506	3.19E-03
IN12050 5_4	3522	4.07	87.2	1.577	0.067	0.310	0.00082	0.466	5.38E-03
IN12050 5_2	2776	6.07	75.5	2.459	0.113	0.194	0.00072	0.797	6.31E-03
IN12050 5_1	2908	9.43	50.7	3.461	0.125	0.210	0.00122	0.839	2.01E-02
IN12053 5_1	2209	12.3	61.4	3.986	0.150	0.139	0.00098	1.368	1.06E-02
IN12053 5_5	2293	5.79	60.2	3.891	0.133	0.145	0.00049	0.553	3.66E-03
IN12053 5_6	2426	8.62	67.2	3.257	0.139	0.157	0.00080	1.718	9.77E-03
IN12053 5_9	3694	9.13	71.6	1.804	0.066	0.347	0.00208	0.197	3.48E-03
IN12053 5_10	3582	8.84	69.7	1.931	0.080	0.323	0.00185	0.860	9.10E-03
IN12053 5_17	2059	6.49	59.7	4.454	0.167	0.127	0.00047	0.119	9.45E-04
IN12053 5_9_2	2312	4.44	67.8	3.416	0.111	0.147	0.00038	0.042	6.84E-04
IN12053 6_7	3361	10.3	86.9	1.682	0.093	0.280	0.00184	0.554	1.05E-02
IN12053 6_6	3371	9.53	88.8	1.639	0.077	0.281	0.00172	1.470	1.89E-02
IN12053 7_1	3364	7.96	82.0	1.779	0.074	0.280	0.00143	0.773	1.14E-02
IN12053 7_3	3338	13.1	84.7	1.740	0.096	0.276	0.00231	1.021	1.46E-02
IN12053 7_9	2722	7.96	76.3	2.494	0.090	0.188	0.00091	0.639	9.94E-03
IN12054 4_1	2580	7.82	89.0	2.284	0.082	0.172	0.00081	0.092	1.06E-03
IN12054 4_2	2483	6.39	86.2	2.470	0.088	0.163	0.00062	0.894	6.85E-03
IN12054 4_4	2559	16.4	78.3	2.622	0.093	0.170	0.00167	0.279	4.05E-03
IN12054 4_6	2696	7.52	94.7	2.035	0.073	0.185	0.00084	1.227	9.76E-03
IN12054 4_7	3175	7.32	92.8	1.692	0.066	0.249	0.00115	0.228	3.23E-03
IN12054 3_1	2921	8.94	101.5	1.719	0.075	0.212	0.00117	0.437	6.41E-03
IN12054 3_1_2	3431	6.17	96.8	1.471	0.052	0.293	0.00116	0.062	2.49E-03
IN12054 3_3	2754	6.98	96.0	1.955	0.077	0.191	0.00081	1.153	7.82E-03
IN12054 3_10	2746	9.01	95.6	1.969	0.087	0.191	0.00104	1.422	3.46E-02
IN12054 3_13	2717	9.88	91.1	2.095	0.086	0.187	0.00112	1.310	1.45E-02
IN12054 1_13	1903	6.72	79.6	3.660	0.132	0.117	0.00044	0.683	3.69E-03
IN12054 1_13_2	2671	6.54	93.3	2.087	0.078	0.182	0.00072	2.123	9.17E-03
IN12054 2_11	2715	7.44	92.6	2.061	0.087	0.187	0.00084	0.933	1.07E-02
IN12054 2_7	2721	9.8	91.2	2.089	0.076	0.188	0.00112	1.112	1.17E-02
IN12054 1_5	2207	13.7	83.5	2.932	0.100	0.138	0.00109	0.946	5.61E-03
IN12054 2_2	2752	7.14	95.6	1.965	0.074	0.191	0.00083	0.766	1.63E-02
IN12054 1_2	2567	10.2	89.4	2.287	0.085	0.171	0.00104	0.686	7.88E-03

Table 3. Data used for zircon trace-element geochemical analysis. Upper two tables of CTG samples, lower two tables of Voizel suite samples.

IN05001

Element	rock	zircon	zircon/rock
		12	12
La	56.100	84.979	1.515
Pr	8.910	12.156	1.364
Nd	30.090	37.504	1.246
Sm	4.737	5.717	1.207
Gd	3.830	39.035	10.192
Tb	0.570	3.504	6.148
Dy	3.450	37.492	10.867
Ho	0.690	14.815	21.471
Er	2.111	73.014	34.587
Tm	0.312	16.922	54.316
Yb	2.113	169.690	80.303
Lu	0.337	42.811	127.129

IN12012

Element	rock	zircon				zircon/rock			
		6_10	6_9	6_5	6_4	6.1	6.9	6.5	6.4
La	32.050	1.454	19.177	3.104	5.781	0.045	0.598	0.097	0.180
Pr	6.701	1.516	12.819	4.018	4.899	0.226	1.913	0.600	0.731
Nd	24.850	14.835	83.382	35.913	38.155	0.597	3.355	1.445	1.535
Sm	4.549	13.787	24.906	20.851	19.734	3.031	5.475	4.584	4.338
Gd	3.475	54.521	57.879	58.888	54.258	15.689	16.656	16.946	15.614
Tb	0.492	17.782	12.862	16.661	13.542	36.143	26.143	33.863	27.524
Dy	2.868	180.511	134.654	165.362	137.124	62.940	46.950	57.658	47.812
Ho	0.544	67.687	49.180	57.442	49.503	124.424	90.405	105.593	90.998
Er	1.550	281.629	206.423	239.772	208.337	181.696	133.176	154.692	134.411
Tm	0.232	57.575	42.207	47.525	41.210	248.167	181.926	204.851	177.627
Yb	1.578	465.280	356.486	394.791	345.210	294.854	225.910	250.184	218.764
Lu	0.251	103.987	77.566	86.061	76.623	414.293	309.028	342.873	305.270

IN12027

Element	rock	zircon			zircon/rock		
		4_4	4_4_2	4_1	4.4	4.4.2	4.1
La	10.930	1.473	2.430	50.096	0.135	0.222	4.583
Pr	2.058	1.953	2.595	40.191	0.949	1.261	19.529
Nd	7.457	12.334	13.915	231.595	1.654	1.866	31.057
Sm	1.508	8.915	7.475	123.778	5.912	4.957	82.081
Gd	1.436	21.534	20.057	205.124	14.996	13.967	142.844
Tb	0.216	6.676	5.680	40.685	30.909	26.295	188.358
Dy	1.334	66.528	61.409	314.845	49.871	46.034	236.016
Ho	0.263	25.000	25.162	94.026	95.056	95.674	357.513
Er	0.740	118.473	125.918	367.622	160.098	170.160	496.786
Tm	0.117	26.637	31.548	75.063	227.663	269.642	641.567
Yb	0.749	244.245	297.511	669.412	326.094	397.211	893.741
Lu	0.125	58.730	74.267	151.497	469.841	594.138	1211.979

IN12046

Element	rock	zircon				zircon/rock			
		5_15	4_2	4_8	4_16	5.15	4.2	4.8	4.16
La	52.670	13.017	183.261	0.082	38.091	0.247	3.479	0.002	0.723
Pr	9.001	6.633	59.544	0.084	16.000	0.737	6.615	0.009	1.778
Nd	28.440	36.969	210.840	1.117	91.353	1.300	7.413	0.039	3.212
Sm	4.077	14.823	16.697	2.263	17.211	3.636	4.096	0.555	4.221
Gd	3.243	36.983	121.202	13.110	48.379	11.404	37.374	4.043	14.918
Tb	0.435	10.216	11.949	5.416	8.076	23.485	27.470	12.450	18.566
Dy	2.352	122.763	143.864	71.225	98.208	52.195	61.166	30.283	41.755
Ho	0.445	56.284	59.176	32.838	41.123	126.482	132.979	73.794	92.412
Er	1.265	296.583	281.646	174.835	203.762	234.453	222.645	138.210	161.077
Tm	0.181	76.206	66.458	44.574	48.189	421.026	367.170	246.267	266.236
Yb	1.218	781.421	601.580	437.420	451.486	641.561	493.908	359.130	370.679
Lu	0.188	196.011	141.710	111.932	106.036	1042.612	753.777	595.385	564.022